gross tumors (defined as having a largest measured diameter of >3 mm) in the peritoneal cavity, whereas only 40% of MT-1-inoculated animals demonstrated gross tumor formation. In fact, control mice that were injected with MT-1 primarily formed very small disseminated masses, rather than gross tumors, within the peritoneal cavity. However, the origin of these masses could not be identified because we could not detect either the HTLV-I *tax* or human *β-globin* genes by PCR due to the small amount of genomic DNA available.

The TL-Om1 cell line was chosen for further analysis of the anti-tumor effects of DHMEQ because 100% of TL-Om1-inoculated NOD/SCID $\beta 2m^{null}$ mice formed gross tumors in the peritoneal cavity. We showed that DHMEQ suppressed the growth of transplanted cells in NOD/SCID $\beta 2m^{null}$ mice injected with TL-Om1 cells subcutaneously, in contrast to the significant increase in tumor burden observed in non-treated mice. Furthermore, apoptotic cells were present in tumors from DHMEQ-treated mice, similar to that reported for Tax-expressing HTLV-I-transformed cells [21]. Although mice injected subcutaneously with HUT-102 cells have been shown to form tumors at the inoculation site and have shown infiltration of inoculated cells into various organs [22], we could not detect the infiltration of TL-Om1 cells into other organs in either DHMEQ-treated or non-treated mice inoculated with TL-Om1 cells subcutaneously. This discrepancy is probably due to tumor volume at the inoculation site, because we found little difference in infiltration of these cells via intraperitoneal injection in each mouse model [21]. However, this system was useful for directly measuring response to DHMEQ in vivo and for detecting apoptosis.

In conclusion, DHMEQ significantly prevented the growth of tumors resulting from injection of Tax-deficient HTLV-I-infected cells in NOD/SCID $\beta 2m^{null}$ mice. Combined with previous studies, these results indicate that DHMEQ has strong potential for ATL therapy, regardless of whether Tax expression can be detected. In addition, our data provide a more extensive analysis of an NF-κB inhibitor predicted to act as an ATL chemotherapeutic agent in vivo than any other study to date.

Acknowledgements

This work was supported in part by a Grant-in-Aid for Scientific Research from the Japan Society for the Promotion of Science. We thank Dr. Toru Urano for helpful discussions, Noboru Sakio and Noriyuki Sakamoto for animal care, and Yoshiteru Tanaka for technical assistance. The anti-Tax/HTLV-I Tax hybridoma 168A51-42 (Tab176) was obtained from Dr. Beatrice C. Langton through the AIDS Research and Reference Reagent Program, Division of AIDS, NIAID, NIH (Bethesda, MD).

References

[1] B.J. Poiesz, F.W. Ruscetti, A.F. Gazdar, P.A. Bunn, J.D. Minna, R.C. Gallo, Detection and isolation of type C retrovirus particles from fresh and cultured lymphocytes of a patient with cutaneous T cell lymphoma, Proc. Natl. Acad. Sci. USA 77 (1980) 7415–7419.

[2] Y. Hinuma, K. Nagata, M. Hanaoka, M. Nakai, T. Matsumoto, K.I. Kinoshita, et al., Adult T cell leukemia: antigen in an ATL cell line and detection of antibodies to the antigen in human sera, Proc. Natl. Acad. Sci. USA 78 (1981) 6476–6480.

[3] T. Watanabe, HTLV-I-associated diseases, Int. J. Hematol. 66 (1997) 257–278.

[4] Y. Yamada, M. Tomonaga, H. Fukuda, S. Hanada, A. Utsunomiya, M. Tara, et al., A new G-CSF-supported combination chemotherapy, LSG15, for adult T-cell leukaemia-lymphoma: Japan Clinical Oncology Group Study 9303, Br. J. Haematol. 113 (2001) 375–382.

[5] S. Yamaoka, G. Courtois, C. Bessia, S.T. Whiteside, R. Weil, F. Agou, et al., Complementation cloning of NEMO, a component of the IκB kinase complex essential for NF-κB activation, Cell 93 (1998) 1231–1240.

[6] S.C. Sun, S. Yamaoka, Activation of NF-kB by HTLV-I and implications for cell transformation, Oncogene 24 (2005) 5952–5964.

[7] N. Mori, M. Fujii, S. Ikeda, Y. Yamada, M. Tomonaga, D.W. Ballard, et al., Constitutive activation of NF-κB in primary adult T cell leukemia cells, Blood 93 (1999) 2360–2368.

[8] N. Hironaka, K. Mochida, N. Mori, M. Maeda, N. Yamamoto, S. Yamaoka, Tax-independent constitutive IκB kinase activation in adult T-cell leukemia cells, Neoplasia 6 (2004) 266–278.

[9] M. Watanabe, T. Ohsugi, M. Shoda, T. Ishida, S. Aizawa, M. Maruyama-Nagai, et al., Dual targeting of transformed and untransformed HTLV-1-infected T-cells by DHMEQ, a potent and selective inhibitor of NF-κB, as a strategy for chemoprevention and therapy of adult T cell leukemia, Blood 106 (2005) 2462–2471.

[10] R. Horie, T. Watanabe, K. Umezawa, Blocking NF-κB as a potential strategy to treat adult T-cell leukemia/lymphoma, Drug News Perspect. 19 (2006) 201–209.

[11] K. Umezawa, Inhibition of tumor growth by NF-κB inhibitors, Cancer Sci. 97 (2006) 990–995.

[12] N. Matsumoto, H. Iinuma, T. Sawa, T. Takeuchi, S. Hirano, T. Yoshioka, et al., Epoxyquinomicins A, B, C and D, new antibiotics from Amycolatopsis. II. Effect on type II collagen-induced arthritis in mice, J. Antibiot. (Tokyo) 50 (1997) 906–911.

[13] N. Matsumoto, A. Ariga, S. To-e, H. Nakamura, N. Agata, S. Hirano, et al., Synthesis of NF-κB activation inhibitors

derived from epoxyquinomicin C, Bioorg. Med. Chem. Lett. 10 (2000) 865–869.
[14] A. Ariga, J. Namekawa, N. Matsumoto, J. Inoue, K. Umezawa, Inhibition of tumor necrosis factor-α-induced nuclear translocation and activation of NF-κB by dehydroxymethylepoxyquinomicin, J. Biol. Chem. 277 (2002) 24625–24630.
[15] E. Kikuchi, Y. Horiguchi, J. Nakashima, K. Kuroda, M. Oya, T. Ohigashi, et al., Suppression of hormone-refractory prostate cancer by a novel nuclear factor κB inhibitor in nude mice, Cancer Res. 63 (2003) 107–110.
[16] D.V. Starenki, H. Namba, V.A. Saenko, A. Ohtsuru, S. Maeda, K. Umezawa, et al., Induction of thyroid cancer cell apoptosis by a novel nuclear factor κB inhibitor, dehydroxymethylepoxyquinomicin, Clin. Cancer Res. 10 (2004) 6821–6829.
[17] G. Matsumoto, M. Muta, K. Umezawa, T. Suzuki, K. Misumi, K. Tsuruta, et al., Enhancement of the caspase-independent apoptotic sensitivity of pancreatic cancer cells by DHMEQ, an NF-κB inhibitor, Int. J. Oncol. 27 (2005) 1247–1255.
[18] M. Watanabe, M.Z. Dewan, T. Okamura, M. Sasaki, K. Itoh, M. Higashihara, et al., A Novel NF-κB inhibitor DHMEQ selectively targets constitutive NF-κB activity and induces apoptosis of multiple myeloma cells in vitro and in vivo, Int. J. Cancer 114 (2005) 32–38.
[19] H. Tatetsu, Y. Okuno, M. Nakamura, F. Matsuno, T. Sonoki, I. Taniguchi, et al., Dehydroxymethylepoxyquinomicin, a novel nuclear factor-κB inhibitor, induces apoptosis in multiple myeloma cells in an IκBα-independent manner, Mol. Cancer Ther. 4 (2005) 1114–1120.
[20] G. Matsumoto, J. Namekawa, M. Muta, T. Nakamura, H. Bando, K. Tohyama, et al., Targeting of nuclear factor κB pathways by dehydroxymethylepoxyquinomicin, a novel inhibitor of breast carcinomas: antitumor and antiangiogenic potential in vivo, Clin. Cancer Res. 11 (2005) 1287–1293.
[21] T. Ohsugi, R. Horie, T. Kumasaka, A. Ishida, T. Ishida, K. Yamaguchi, et al., In vivo antitumor activity of the NF-kB inhibitor dehydroxymethylepoxyquinomicin in a mouse model of adult T-cell leukemia, Carcinogenesis 26 (2005) 1382–1388.
[22] T. Ohsugi, T. Kumasaka, A. Ishida, T. Ishida, R. Horie, T. Watanabe, et al., In vitro and in vivo antitumor activity of the NF-κB inhibitor DHMEQ in the human T-cell leukemia virus type I-infected cell line, HUT-102, Leukemia Res. 30 (2006) 90–97.
[23] S.W. Christianson, D.L. Greiner, R.A. Hesselton, J.H. Leif, E.J. Wagar, I.B. Schweitzer, et al., Enhanced human CD4+ T cell engraftment in β2-microglobulin-deficient NOD-scid mice, J. Immunol. 158 (1997) 3578–3586.
[24] K. Sugamura, M. Fujii, M. Kannagi, M. Sakitani, M. Takeuchi, Y. Hinuma, Cell surface phenotypes and expression of viral antigens of various human cell lines carrying human T-cell leukemia virus, Int. J. Cancer 34 (1984) 221–228.
[25] I. Miyoshi, I. Kubonishi, S. Yoshimoto, T. Akagi, Y. Ohtsuki, Y. Shiraishi, et al., Type C virus particles in a cord T-cell line derived by co-cultivating normal human cord leukocytes and human leukaemic T-cells, Nature 294 (1981) 770–771.
[26] T. Ohsugi, K. Kumasaka, T. Urano, Construction of a full-length human T cell leukemia virus type I (HTLV-I) genome from MT-2 cells containing multiple defective proviruses using overlapping polymerase chain reaction, Anal. Biochem. 329 (2004) 281–288.
[27] Y. Satou, K. Nosaka, Y. Koya, JI. Yasunaga, S. Toyokuni, M. Matsuoka, Proteasome inhibitor, bortezomib, potently inhibits the growth of adult T-cell leukemia cells both in vivo and in vitro, Leukemia 18 (2004) 1357–1363.
[28] T. Kinoshita, M. Shimoyama, K. Tobinai, M. Ito, S. Ito, S. Ikeda, et al., Detection of mRNA for the tax1/rex1 gene of human T-cell leukemia virus type I in fresh peripheral blood mononuclear cells of adult T-cell leukemia patients and viral carriers by using the polymerase chain reaction, Proc. Natl. Acad. Sci. USA 86 (1989) 5620–5624.
[29] Y. Furukawa, M. Osame, R. Kubota, M. Tara, M. Yoshida, Human T-cell leukemia virus type-1 (HTLV-1) Tax is expressed at the same level in infected cells of HTLV-1-associated myelopathy or tropical spastic paraparesis patients as in asymptomatic carriers but at a lower level in adult T-cell leukemia cells, Blood 85 (1995) 1865–1870.

MOLECULAR AND CELLULAR BIOLOGY, Dec. 2007, p. 8190–8204 Vol. 27, No. 23
0270-7306/07/$08.00+0 doi:10.1128/MCB.00661-07

Extracellular Signal-Regulated Kinase/Mitogen-Activated Protein Kinase Regulates Actin Organization and Cell Motility by Phosphorylating the Actin Cross-Linking Protein EPLIN▽†

Mei-Ying Han,[1,2] Hidetaka Kosako,[1]* Toshiki Watanabe,[2] and Seisuke Hattori[1,3]

Division of Cellular Proteomics (BML), The Institute of Medical Science,[1] and Department of Medical Genome Sciences, Graduate School of Frontier Sciences,[2] The University of Tokyo, 4-6-1 Shirokanedai, Minato-ku, Tokyo 108-8639, Japan, and Department of Biochemistry, School of Pharmaceutical Sciences, Kitasato University, 5-9-1 Shirokane, Minato-ku, Tokyo 108-8641, Japan[3]

Received 16 April 2007/Returned for modification 11 June 2007/Accepted 7 September 2007

Extracellular signal-regulated kinase (ERK) is important for various cellular processes, including cell migration. However, the detailed molecular mechanism by which ERK promotes cell motility remains elusive. Here we characterize epithelial protein lost in neoplasm (EPLIN), an F-actin cross-linking protein, as a novel substrate for ERK. ERK phosphorylates Ser360, Ser602, and Ser692 on EPLIN in vitro and in intact cells. Phosphorylation of the C-terminal region of EPLIN reduces its affinity for actin filaments. EPLIN colocalizes with actin stress fibers in quiescent cells, and stimulation with platelet-derived growth factor (PDGF) induces stress fiber disassembly and relocalization of EPLIN to peripheral and dorsal ruffles, wherein phosphorylation of Ser360 and Ser602 is observed. Phosphorylation of these two residues is also evident during wound healing at the leading edge of migrating cells. Moreover, expression of a non-ERK-phosphorylatable mutant, but not wild-type EPLIN, prevents PDGF-induced stress fiber disassembly and membrane ruffling and also inhibits wound healing and PDGF-induced cell migration. We propose that ERK-mediated phosphorylation of EPLIN contributes to actin filament reorganization and enhanced cell motility.

Extracellular signal-regulated kinase (ERK), a member of the mitogen-activated protein kinase (MAPK) family, plays pivotal roles in diverse cellular events, such as proliferation, differentiation, migration, growth, and survival (4, 18, 30, 44). Activation of ERK occurs in response to growth factor stimulation through the Ras-Raf-MEK pathway, and activated ERK translocates from the cytoplasm to the nucleus, where it phosphorylates several protein kinases, nuclear transcription factors, and other proteins (12, 17, 30). In addition to its role in the nucleus, recent data show that ERK is involved as an essential component in the migration of cells from many different organisms (9, 16, 21, 38). Certain substrates, such as myosin light chain kinase (25), focal adhesion kinase (14), paxillin (19), actopaxin (5), calpain (10), and vinexin (24), are known to function in ERK-mediated cell migration (13).

Cell migration requires dynamic reorganization of the actin cytoskeleton (31). Composite extracellular stimuli, including growth factors and cell-matrix adhesions, trigger signals for cell motility, which are then transduced by diverse intracellular components, such as the MAPK family (13, 39), protein kinase B/Akt (36), tyrosine kinases (6), and Rho family small GTPases (8, 34). During dynamic remodeling of the actin system for cell migration, a number of actin cross-linking/bundling proteins are crucial (1, 37, 40, 46). In addition, actin bundles and cross-linked networks play key roles in the generation of tension and flexibility in the actin cytoskeleton (2, 33). Thus, ERK might mediate cell migration via phosphorylating some actin cross-linking/bundling proteins.

Epithelial protein lost in neoplasm (EPLIN) was originally identified as the product of a gene that is transcriptionally down-regulated or lost in a number of human epithelial tumor cells, including oral, prostate, and breast cancer cell lines (3, 22). EPLIN is expressed from a single gene as two isoforms, α and β, the latter of which has an extra N-terminal sequence of 160 amino acids. Both EPLINα and -β contain a centrally located LIM domain that may mediate self-dimerization and N- and C-terminal actin-binding sites flanking the LIM domain (23). EPLIN cross-links and bundles actin filaments, thereby stabilizing actin stress fibers. Furthermore, EPLIN inhibits Arp2/3 complex-mediated branching nucleation of actin filaments. Thus, EPLIN controls actin filament dynamics by stabilizing actin filament networks (23). It is therefore assumed that the loss of EPLIN expression in cancer cells is involved in the enhanced motility of these cells.

Recently, we identified EPLIN as a candidate substrate for ERK by a proteomic approach using two-dimensional difference gel electrophoresis (2D-DIGE) combined with phosphoprotein enrichment. In this study, we show that ERK phosphorylates EPLIN in vitro and in vivo. Phosphorylation of the C-terminal region of EPLIN inhibits its actin-binding activity. Stimulation with platelet-derived growth factor (PDGF) induces stress fiber disassembly and localization of phosphorylated EPLIN to peripheral and dorsal ruffles. Furthermore, expression of a non-ERK-phosphorylatable mutant of EPLIN

* Corresponding author. Mailing address: Division of Cellular Proteomics (BML), The Institute of Medical Science, The University of Tokyo, 4-6-1 Shirokanedai, Minato-ku, Tokyo 108-8639, Japan. Phone and fax: 81-3-6409-2073. E-mail: kosako@ims.u-tokyo.ac.jp.

† Supplemental material for this article may be found at http://mcb.asm.org/.

▽ Published ahead of print on 17 September 2007.

prevents PDGF-induced membrane ruffling as well as cell migration. These results suggest that phosphorylation of EPLIN by ERK leads to reorganization of actin filaments and stimulation of cell motility.

MATERIALS AND METHODS

Cell culture and transfection. ΔB-Raf:ER cells (NIH 3T3 cells expressing the B-Raf kinase domain fused to the estrogen receptor ligand binding domain) (32) were cultured in Dulbecco's modified Eagle's medium (DMEM) without phenol red (Invitrogen, Carlsbad, CA) but containing 10% fetal bovine serum (FBS). NIH 3T3 cells were cultured in DMEM containing 10% calf serum (CS). 293T and HeLa cells were cultured in DMEM containing 10% FBS. Primary calvarial osteoblasts were isolated from 1-day-old Jc1:ICR mice by five sequential digestions (for 10 min each) with 0.1% collagenase and 0.2% dispase. The cells from the last four digestions were grown in α-minimum essential medium (Invitrogen) containing 10% FBS. Transfections were performed by using Lipofectamine 2000 (Invitrogen) for 293T and ΔB-Raf:ER cells and Lipofectamine LTX (Invitrogen) for NIH 3T3 and osteoblastic cells, according to the manufacturer's instructions.

Plasmids and protein expression. The DNA fragments encoding mouse EPLINα (161-753), EPLINβ (1-753), EPLIN-N (161-387), and EPLIN-C (440-753) were amplified by PCR and cloned into pCMV-Tag3-Myc (Stratagene, La Jolla, CA), pCMV-Tag2-Flag (Stratagene), or pGEX-4T-3 vector (GE Healthcare, Buckinghamshire, United Kingdom). For expression of enhanced green fluorescent protein (EGFP)-fused EPLINα in mammalian cells, the DNA fragment encoding EGFP was amplified by PCR and cloned into the C-terminal coding region of pCMV-Tag3-Myc-EPLINα. Point mutations were introduced using a QuikChange site-directed mutagenesis kit (Stratagene) according to the manufacturer's instructions.

Antibodies and reagents. A rabbit polyclonal antibody (PAb) against mouse EPLIN was generated against glutathione *S*-transferase (GST)-fused full-length EPLINα expressed in *Escherichia coli* BL21-CodonPlus (DE3)-RIPL (Stratagene) and was affinity purified with immobilized EPLINα, from which the GST moiety was removed by thrombin digestion. Anti-phosphorylated-EPLIN antibodies were raised by immunizing rabbits with keyhole limpet hemocyanin-conjugated synthetic phosphopeptides corresponding to 11-amino-acid sequences of EPLINα and were purified from antiserum as the bound fraction of a phosphopeptide-conjugated SulfoLink column (Pierce, Rockford, IL) and the unbound fraction of a non-phosphopeptide-conjugated column. The following antibodies were also used: anti-Myc mouse monoclonal antibody (MAb) 9E10, anti-Myc rabbit PAb A-14, anti-ERK1 rabbit PAb K-23 (Santa Cruz Biotechnology, Santa Cruz, CA), anti-p-ERK mouse MAb E10, anti-p-RSK (Thr573) rabbit PAb (Cell Signaling Technology, Danvers, MA), antiactin mouse MAb (Chemicon, Temecula, CA), anti-Flag mouse MAb M2 (Sigma, St. Louis, MO), anti-EPLIN rabbit PAb BL1141 (Bethyl, Montgomery, TX), anti-GFP rabbit PAb (Invitrogen), and antihemagglutinin (anti-HA) rat MAb 3F10 (Roche, Basel, Switzerland). PDGF and 4-hydroxy-tamoxifen (4-HT) were obtained from Sigma. U0126 was purchased from Promega (Madison, WI).

Phosphatase treatment. Myc-EPLINβ was transfected into ΔB-Raf:ER cells. Cells were then treated with 4-HT for 2 h, and cell lysates were immunoprecipitated with an anti-Myc (9E10) antibody. Immunoprecipitates were resuspended in a reaction buffer containing 4 units of calf intestinal alkaline phosphatase (CIAP; Takara, Shiga, Japan) and incubated at 37°C for 60 min. The reaction was stopped by adding Laemmli's sample buffer and boiling the samples. Proteins were separated by sodium dodecyl sulfate-polyacrylamide gel electrophoresis (SDS-PAGE) and subjected to immunoblotting with an anti-Myc (A-14) antibody.

RNAi and rescue assays. EPLIN small interfering RNA (siRNA) and siCONTROL nontargeting siRNA 1 were obtained from Dharmacon (Lafayette, CO). The sequences of siRNA duplexes that target mouse EPLIN are as follows: sense, 5′-GGACGAAUCUACUGUAAGCUU-3′; and antisense, 5′-GCUUACAGUAGAUUCGUCCUU-3′. ERK1 and ERK2 Stealth siRNA duplexes were obtained from Invitrogen. The sequences of mouse ERK1 siRNAs are as follows: sense, 5′-GGAAGCCAUGAGAGAUGUUUACAUU-3′; and antisense, 5′-AAUGUAAACAUCUCUCAUGGCUUCC-3′. The sequences of mouse ERK2 siRNAs are as follows: sense, 5′-GGCUAAAGUAUAUCCAUUCAGCUAA-3′; and antisense, 5′-UUAGCUGAAUGGAUAUACUUUAGCC-3′. These siRNA duplexes were transfected into NIH 3T3 or primary osteoblastic cells by using DharmaFECT 1 reagent (Dharmacon), and cells were cultured for 72 h. For rescue assays, we constructed an RNA interference (RNAi)-refractory EPLINα cDNA (EPLINαr) and EPLINα(S360/602/692A) cDNA [EPLINαr(S360/602/692A)]. Three silent mutations were introduced into the mouse EPLINα and EPLINα(S360/602/692A) cDNAs, changing the nucleotide sequence at positions 817 to 825 of EPLINα/EPLINα(S360/602/692A) to CG CATATAT.

In vitro kinase assay. Phosphorylation of recombinant GST-EPLINα, GST–EPLIN-N, GST–EPLIN-C, and their Ala substitutes by ERK was performed by incubation of 50 ng of recombinant active ERK2 (New England Biolabs, Beverly, MA) with 3.0 μg each of GST-EPLINα, -N, -C, and their mutants and 50 μM [γ-^{32}P]ATP (2.5 μCi; GE Healthcare) in 30 μl of a kinase buffer (50 mM Tris-HCl, pH 7.5, 15 mM $MgCl_2$, 1 mM EGTA, and 2 mM dithiothreitol [DTT]) for 20 min at 30°C. The reaction was stopped by adding Laemmli's sample buffer and boiling the samples. Half of the sample was subjected to 10% SDS-PAGE, and the phosphorylation reaction was visualized by autoradiography.

LC-tandem mass spectrometry (LC-MS/MS) analysis. GST-EPLINα phosphorylated by ERK in vitro was separated by SDS-PAGE. In-gel digestion was performed using sequencing-grade trypsin (Promega) or endoproteinase Glu-C (Roche). The resulting peptides were separated by C_{18} reversed-phase high-pressure liquid chromatography (LC), and each peptide was analyzed with a matrix-assisted laser desorption ionization–time-of-flight tandem mass spectrometer (model 4700 proteomics analyzer; Applied Biosystems, Foster City, CA). Detected masses and peptide sequences were subjected to database searches with the Mascot search engine (Matrix Science, London, United Kingdom).

Actin cosedimentation assays. Binding of EPLIN to F-actin was tested in a cosedimentation assay as described previously (23). Briefly, rabbit muscle G-actin (Cytoskeleton, Denver, CO) and GST–EPLIN-C or GST–EPLIN-C(S602/692A) were separately precleared by centrifugation at 100,000 × *g* for 30 min at 4°C. G-actin (2.5 μM) was polymerized in 5 mM Tris-HCl, pH 7.5, 100 mM KCl, 2 mM $MgCl_2$, 0.2 mM ATP, and 0.5 mM DTT at room temperature for 30 min. Fifty microliters of F-actin was then incubated with 10 μl of ERK-phosphorylated or nonphosphorylated GST–EPLIN-C or GST–EPLIN-C(S602/692A) for 30 min at 4°C. After being centrifuged at 100,000 × *g* for 30 min at 4°C, the supernatant and pellet were separated and analyzed by SDS-PAGE and Coomassie brilliant blue (CBB) staining.

Immunoprecipitation. Cells were lysed with immunoprecipitation buffer (20 mM Tris-HCl, pH 7.5, 150 mM NaCl, 10 mM NaF, 25 mM β-glycerophosphate, 2 mM EGTA, 2 mM $MgCl_2$, 1% NP-40, 10% glycerol, 1 mM phenylmethylsulfonyl fluoride, 20 μg/ml aprotinin, and 2 mM DTT) for 15 min on ice. Lysates were clarified by centrifugation and incubated with agarose beads conjugated with the 9E10 anti-Myc antibody for 1 h at 4°C. The beads were then washed three times with immunoprecipitation buffer and finally resuspended in Laemmli's sample buffer. Proteins were resolved by SDS-PAGE for immunoblot analysis.

Immunofluorescence microscopy. Cells were grown on coverslips coated with poly-L-lysine and fixed with 3.7% formaldehyde for 10 min at room temperature. Fixed cells were then permeabilized with 0.1% Triton X-100 for 10 min. After being washed with phosphate-buffered saline, the cells were incubated with primary antibodies in phosphate-buffered saline containing 2% goat serum for 2 h, followed by incubation with Alexa Fluor-conjugated secondary antibodies (1:1,000 dilution; Invitrogen) for 1 h. F-actin was detected by staining with rhodamine-phalloidin or Alexa Fluor 647-conjugated phalloidin (Invitrogen). Samples were observed on an inverted microscope (model IX71; Olympus, Tokyo, Japan) equipped with a PlanApo 60×, 1.4-numerical-aperture (NA) oil immersion objective. Images were obtained with a cooled charge-coupled device camera (ORCA-ER; Hamamatsu Photonics, Shizuoka, Japan) controlled by Aqua-Lite software (Hamamatsu Photonics) and were processed using Adobe Photoshop CS3.

Boyden chamber assay. Cell migration was assayed in Boyden chambers (8.0-μm-pore-size polyethylene terephthalate membrane with Falcon cell culture insert; Becton Dickinson, Mountain View, CA) as previously described (7). NIH 3T3 cells transfected with EGFP, EPLINα-EGFP, or EPLINα(S360/602/692A)-EGFP were serum starved with DMEM containing 0.2% CS and then trypsinized and counted. Cells (5×10^4 to 10×10^4) in DMEM containing 0.2% CS (0.8 ml) were added to the upper chamber, and 1.8 ml of appropriate medium, with or without 30 ng/ml PDGF, was added to the lower chamber. When the MEK inhibitor was used in this assay, cells were treated with 20 μM U0126 for 30 min before trypsinization, and U0126 was also added to both the upper and lower chambers during migration. For RNAi rescue assays, cells were sequentially transfected with control siRNA or EPLIN siRNA and EGFP, EPLINαr-EGFP, or EPLINαr(S360/602/692A)-EGFP. For primary osteoblasts, α-minimum essential medium with 0.2% FBS was used. Transwells were incubated for 6 h at 37°C. EGFP-positive cells on both sides of the membrane were counted, and then cells on the inside of the insert were removed with a cotton swab and EGFP-positive

cells on the underside of the insert were counted. The number of cells in five randomly chosen fields per filter was counted by microscopic examination.

Live imaging. To observe PDGF-induced membrane ruffling, NIH 3T3 cells transfected with EPLINα-EGFP or EPLINα(S360/602/692A)-EGFP were stimulated with 50 ng/ml PDGF for 15 min after time-lapse recording. Time-lapse microscopy was performed using a DeltaVision deconvolution microscope system controlled by softWoRx software (Applied Precision, Issaquah, WA) configured around an Olympus IX70 inverted microscope. Images were acquired using a UPlanSApo 20×, 0.85-NA oil immersion objective. For wound-healing assays, after scratching of a monolayer of NIH 3T3 cells transfected with EPLINα-EGFP or EPLINα(S360/602/692A)-EGFP, live cells were recorded at 37°C in a 5% CO_2 atmosphere, using a confocal microscope (CSU22; Yokogawa, Tokyo, Japan) equipped with a cooled charge-coupled device camera (DV887DCS-BV; Andor Technology, Belfast, Northern Ireland). Images were acquired using a UPlanApo 20×, 0.80-NA oil immersion objective and were analyzed with MetaMorph software (Molecular Devices, Downingtown, PA).

RESULTS

ERK-mediated phosphorylation of EPLIN in living cells. To globally identify protein kinase substrates, we recently developed a system consisting of phosphoprotein purification by immobilized metal-affinity chromatography, fluorescent 2D-DIGE, and MS protein identification (20, 41). We applied this method to the ERK signaling pathway and identified 24 candidates for novel ERK targets, one of which was EPLIN (H. Kosako, N. Yamaguchi, M. Ushiyama, E. Nishida, and S. Hattori, submitted for publication).

To examine whether EPLIN is phosphorylated by ERK in living cells, Myc-tagged EPLIN was expressed in ΔB-Raf:ER cells. This cell line is a derivative of NIH 3T3 cells in which the protein kinase domain of mouse B-Raf is expressed as a fusion protein with the hormone-binding domain of the human estrogen receptor (32). ERK can be activated by 4-HT, an antagonist of estrogen. To suppress the ERK pathway, the MEK inhibitor U0126 was used. The lysates of these cells were subjected to immunoblotting with anti-Myc antibody (Fig. 1A, left panel). Both Myc-EPLINα and Myc-EPLINβ showed mobility shifts on SDS-PAGE upon treatment with 4-HT compared to treatment with U0126. To confirm phosphorylation as the cause of these shifts, we examined the effect of phosphatase treatment. Myc-EPLINβ was immunoprecipitated from 4-HT-treated ΔB-Raf:ER cells, and the immunoprecipitates were incubated with CIAP. As shown in Fig. 1A (right panel), the 4-HT-induced band shift of Myc-EPLINβ was completely reversed by CIAP treatment. These results suggest that EPLIN is phosphorylated by the activation of the ERK pathway. To determine the phosphorylation site on EPLIN that induces the mobility shift, HA-tagged wild-type EPLINβ and two Ser-to-Ala mutants were expressed in ΔB-Raf:ER cells, and then the cells were treated with 4-HT or U0126. HA-EPLINβ-S360A did not show the mobility shift (see Fig. S1 in the supplemental material), indicating that the shift was due to the phosphorylation of Ser360 (see below).

We generated a polyclonal antibody by immunizing a rabbit with bacterially expressed full-length mouse EPLINα fused to GST. To examine the specificity of the generated antibody, Flag-tagged EPLIN was expressed in NIH 3T3 cells. Both Flag-EPLINα and Flag-EPLINβ were detected by immunoblotting with our anti-EPLIN, commercially available anti-EPLIN (BL1141), and anti-Flag antibodies (Fig. 1B). The commercial anti-EPLIN (BL1141) antibody showed very little reactivity to endogenous EPLINα (Fig. 1B, middle panel). In contrast, our affinity-purified anti-EPLIN antibody specifically recognized endogenous EPLINα and also EPLINβ, as a faint band (Fig. 1B, left panel, and C). Since EPLINβ includes the entire sequence of EPLINα, EPLINβ is thought to be expressed at a much lower level than EPLINα in NIH 3T3 cells. When ΔB-Raf:ER cells were treated with 4-HT or when NIH 3T3 cells were stimulated with PDGF for 30 min, endogenous EPLINα and -β were phosphorylated, and this was prevented by pretreatment with U0126 (Fig. 1C).

ERK phosphorylates Ser360, Ser602, and Ser692 on EPLIN in vitro and in vivo. As described in the previous section, EPLIN is phosphorylated upon ERK activation. To test whether EPLIN is a direct substrate of ERK, we prepared GST fusion proteins of full-length EPLINα and the N-terminal and C-terminal portions of EPLINα, as illustrated schematically in Fig. 2A. An in vitro kinase assay was then performed, using recombinant active ERK, [γ-^{32}P]ATP, and recombinant GST-EPLINα, GST–EPLIN-N, and GST–EPLIN-C as substrates. Both GST-EPLINα and GST–EPLIN-C were strongly phosphorylated by ERK, whereas GST–EPLIN-N phosphorylation was rather weak (Fig. 2B, lanes 1, 3, and 6). It has been established that ERK preferentially phosphorylates Ser or Thr residues just before Pro residues (11). EPLIN has seven Ser-Pro sequences that are conserved between mouse and human EPLIN proteins (Fig. 2A). To identify ERK phosphorylation sites on EPLIN, we replaced each Ser residue with Ala. As shown in Fig. 2B, lane 4, the S360A substitution completely abolished ERK phosphorylation of EPLIN-N. On the other hand, replacement of either Ser602 or Ser692 by Ala partially abolished phosphorylation, and replacement of both residues (EPLIN-C-S602/692A) markedly reduced phosphorylation (Fig. 2B, lanes 9, 11, and 12). When full-length EPLINα was used as a substrate, replacement of Ser360, Ser602, and Ser692 by Ala (EPLINα-S360/602/692A) strongly impaired phosphorylation by ERK (Fig. 2B, lane 2). This suggests that Ser360, Ser602, and Ser692 are the primary sites at which ERK phosphorylates EPLIN in vitro.

To further confirm the phosphorylation sites, EPLIN phosphorylated by ERK in vitro was digested with trypsin or V8 protease, and the resulting peptides were subjected to LC-MS/MS analysis. As shown in Fig. S2 in the supplemental material, phosphorylation of Ser360, Ser602, and Ser692 was confirmed by this analysis. Phosphorylation of Ser488 and Ser607 was also observed, and these may be minor phosphorylation sites, as suggested by the slightly reduced phosphorylation of EPLIN-C-S488A and -S607A (Fig. 2B, lanes 8 and 10).

We then produced phospho-specific antibodies by using synthetic phosphopeptides that harbor phosphorylated Ser360, Ser602, or Ser692. The anti-pS360 antibody recognized wild-type GST–EPLIN-N and the S372A mutant of GST–EPLIN-N upon ERK-mediated phosphorylation but did not recognize the S360A mutant (Fig. 2C). Similarly, anti-pS602 and anti-pS692 antibodies recognized wild-type and S692A mutant GST-EPLIN-C and wild-type and S602A mutant GST–EPLIN-C, respectively, only when phosphorylated by ERK. These results indicate that the anti-pS360, anti-pS602, and anti-pS692 antibodies specifically recognize EPLIN phosphorylated at Ser360, Ser602, and Ser692, respectively.

To examine whether the anti-pS360, anti-pS602, and anti-

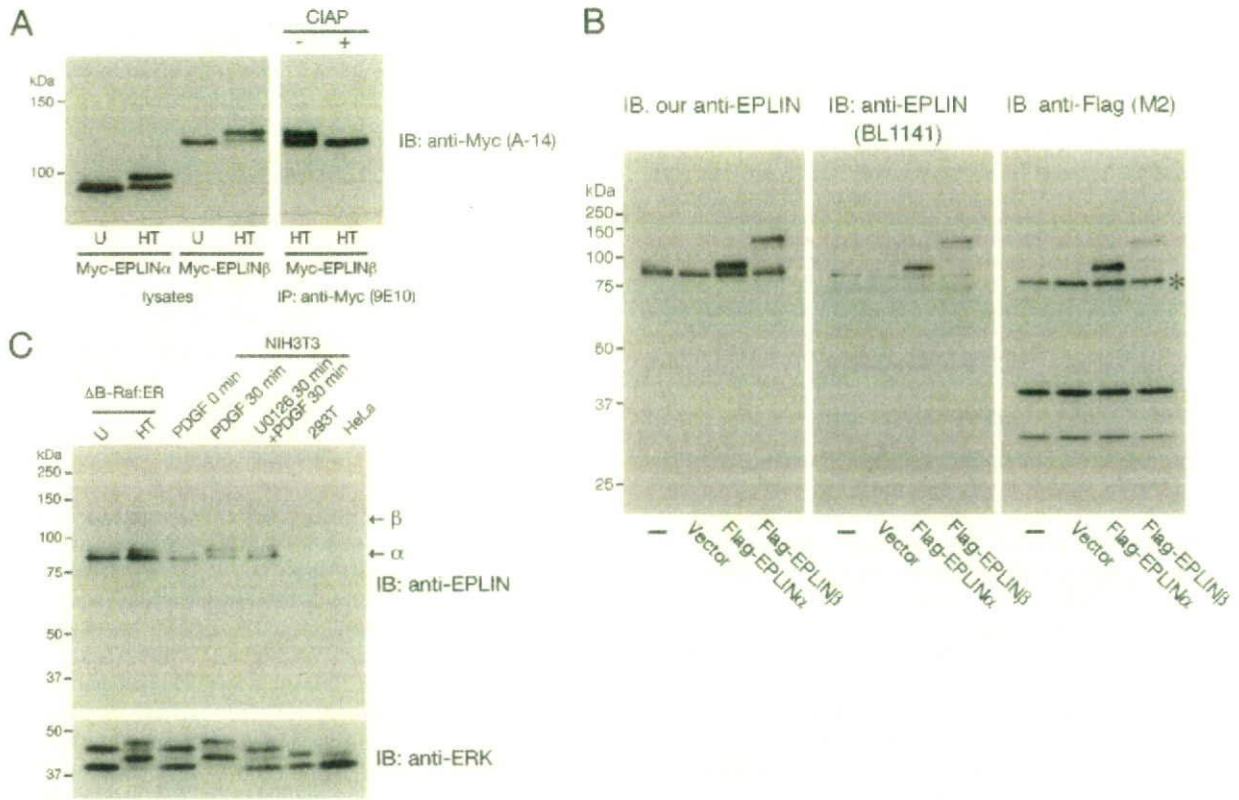

FIG. 1. ERK-mediated phosphorylation of EPLIN in living cells. (A) ΔB-Raf:ER cells transfected with Myc-EPLINα or -β were treated with 20 μM U0126 or 1 μM 4-HT for 2 h, and the lysates were immunoblotted with the A-14 anti-Myc rabbit antibody (left panel). Myc-EPLINβ-transfected cell lysates obtained for the left panel were immunoprecipitated with the 9E10 anti-Myc mouse antibody, and the immunoprecipitates were incubated with or without CIAP (right panel). (B and C) Our affinity-purified anti-mouse EPLIN antibody specifically recognized mouse but not human EPLIN. (B) NIH 3T3 cells were transfected with vector, Flag-EPLINα, or Flag-EPLINβ, as indicated, and immunoblotted with 0.25 μg/ml each of our anti-EPLIN, commercial anti-EPLIN (BL1141), and anti-Flag (M2) antibodies. All panel photos were taken at the same exposure time. The asterisk indicates nonspecific bands that migrated slightly faster than endogenous EPLINα. (C) ΔB-Raf:ER cells were treated with U0126 or 4-HT for 30 min, and serum-starved NIH 3T3 cells were stimulated with 50 ng/ml PDGF for 30 min in the presence or absence of a 30-min pretreatment with U0126. The lysates were immunoblotted with our anti-EPLIN and anti-ERK antibodies. EPLINβ bands became apparent after a longer exposure of the blot (data not shown).

pS692 antibodies can detect endogenous EPLIN phosphorylated by physiological stimuli that activate ERK, immunoblot analysis was performed on lysates from PDGF-stimulated NIH 3T3 cells. As shown in Fig. 2D, after the addition of PDGF, all three antibodies reacted with bands corresponding to EPLINα and EPLINβ. The time course of Ser602 and Ser692 phosphorylation was similar to that of ERK activation, but Ser360 phosphorylation proceeded slowly and increased for up to 240 min. Since the phosphorylation of Ser360 caused the mobility shift, anti-pS602 and anti-pS692 antibodies detected both EPLINα and -β as doublets at later time periods. When immunoblot analysis was performed on lysates from PDGF-stimulated primary calvarial osteoblasts, all three antibodies reacted with bands corresponding to EPLINα (see Fig. 10A). Phosphorylation of these three residues was strongly inhibited by pretreatment with U0126 (Fig. 2D; see Fig. 10A) or transfection with siRNA for ERK2 or ERK1 plus ERK2 (see Fig. 6A). Because the level of ERK2 expression in NIH 3T3 cells is significantly higher than that of ERK1 (note that comparable amounts of ERK1 and ERK2 bands were detected by immunoblotting with the K-23 anti-ERK1 antibody in all figures), it may be reasonable that phosphorylation of EPLIN as well as p90 ribosomal S6 kinase, a well-known ERK substrate, was not clearly inhibited by ERK1 depletion (see Fig. 6A). We therefore concluded that EPLIN is phosphorylated at Ser360, Ser602, and Ser692 by ERK in living cells.

Phosphorylation of the C-terminal region of EPLIN by ERK reduces its affinity for F-actin in vitro and in vivo. Because EPLIN has two actin-binding domains and cross-links actin filaments into bundles (23), we next examined whether phosphorylation of EPLIN regulates its association with F-actin. First, F-actin-binding properties of the nonphosphorylated and ERK-phosphorylated C-terminal region of EPLIN (GST–EPLIN-C) were compared by the F-actin cosedimentation assay in vitro (Fig. 3). In this assay, GST–EPLIN-C preincubated with or without ERK was mixed with purified actin filaments, the sample was ultracentrifuged, and the distribution of GST–EPLIN-C in the supernatant and pellet was examined. GST–EPLIN-C alone did not sediment, indicating that the sedimentation was due to binding to F-actin. The recovery of

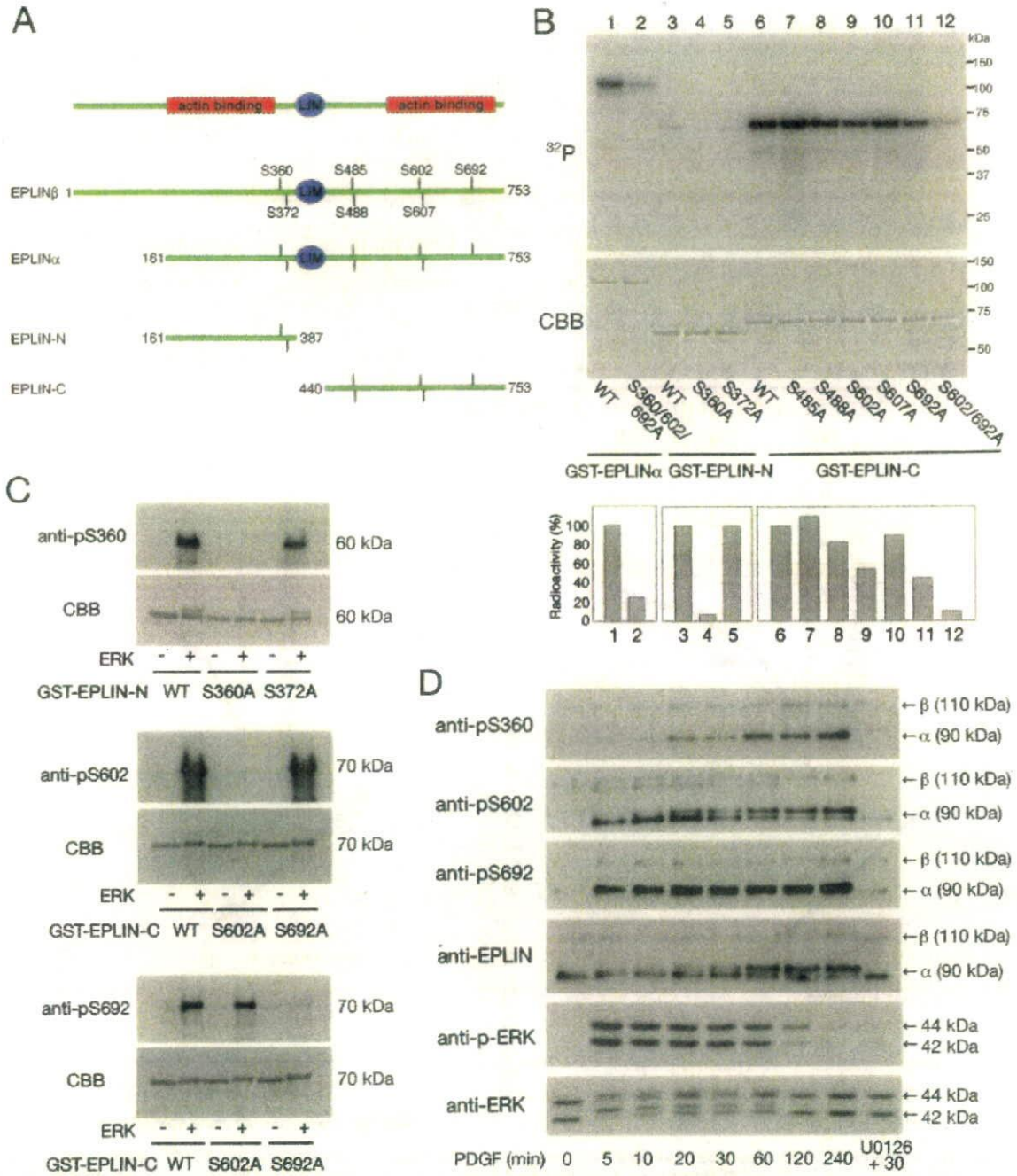

FIG. 2. ERK phosphorylates Ser360, Ser602, and Ser692 of EPLIN. (A) Domain structure of EPLIN and its truncation mutants. Potential ERK phosphorylation sites are indicated. For bacterial expression, EPLINα, EPLIN-N, and EPLIN-C were tagged with GST at the N terminus. (B) An in vitro kinase assay was performed using wild-type (WT) GST-EPLINα, GST–EPLIN-N, GST–EPLIN-C, and their Ser-to-Ala mutants as substrates and recombinant active ERK as a kinase in the presence of [γ-^{32}P]ATP. After electrophoresis, the gel was stained with CBB (middle panel) and subjected to autoradiography (upper panel). The relative intensities of phosphorylated bands were quantified by a Fujix BAS2000 bioimaging analyzer (lower panel). (C) GST–EPLIN-N, GST–EPLIN-C, and their Ala substitutes were incubated with or without ERK in vitro and analyzed by immunoblotting with anti-pS360, anti-pS602, and anti-pS692 antibodies as indicated. (D) Serum-starved NIH 3T3 cells treated with 10 ng/ml PDGF for the indicated times were analyzed by immunoblotting with the indicated antibodies.

ERK-phosphorylated wild-type GST–EPLIN-C in the pellet (35%) was significantly less than that of the nonphosphorylated form (59%), whereas the nonphosphorylatable mutant (S602/692A) of GST–EPLIN-C did not show ERK-dependent changes (63% recovery in the absence of ERK and 62% recovery in its presence) (Fig. 3A). To determine the stoichiometries of binding and dissociation constants (K_ds), various concentrations of these proteins were assayed for cosedimentation with a fixed amount of F-actin. As shown in Fig. 3B, the K_ds of nonphosphorylated and phosphorylated forms of wild-type

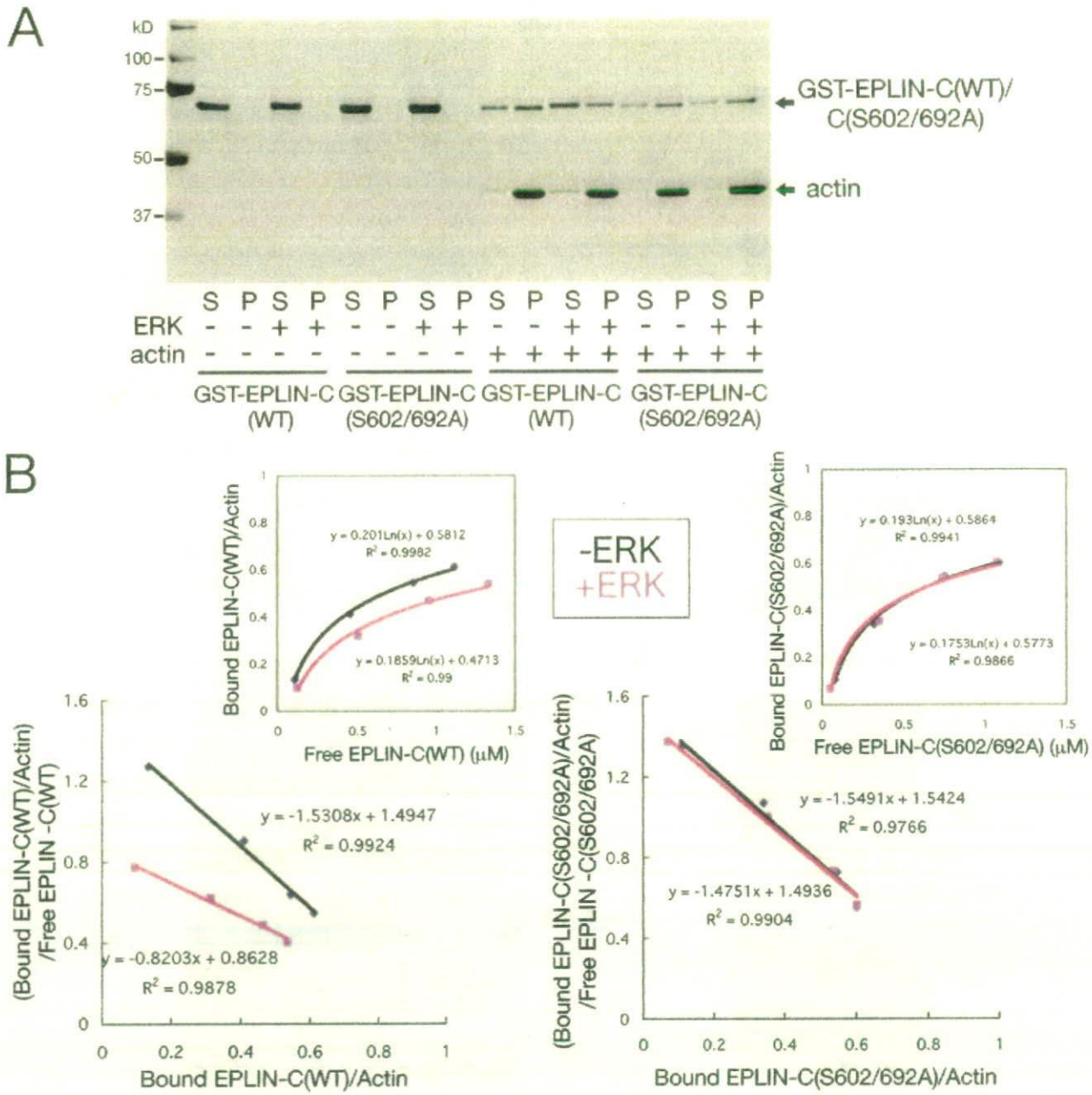

FIG. 3. Phosphorylation of the C-terminal region of EPLIN by ERK reduces its affinity for F-actin in vitro. (A) Phosphorylated (+ERK) or nonphosphorylated (−ERK) GST–EPLIN-C(WT) or GST–EPLIN-C(S602/692A) was mixed with (+) or without (−) 2.5 μM polymerized actin and ultracentrifuged. Supernatants (S) and pellets (P) were analyzed by SDS-PAGE followed by CBB staining. (B) Quantitative analysis of binding of the C-terminal region of EPLIN to actin filaments. The cosedimentation assay was performed by mixing 2.5 μM polymerized actin with various amounts of phosphorylated (red) or nonphosphorylated (black) GST–EPLIN-C(WT) (left panel) or GST–EPLIN-C(S602/692A) (right panel). Amounts of free and bound GST–EPLIN-C in the supernatant and pellet fractions were determined from a digitized CBB-stained gel.

GST–EPLIN-C for F-actin were calculated to be 0.65 μM and 1.2 μM, respectively. On the other hand, GST–EPLIN-C(S602/692A) preincubated with or without ERK showed similar binding properties for F-actin, with K_ds of ~0.6 μM. These results suggest that phosphorylation of the C-terminal region of EPLIN by ERK reduces its affinity for F-actin. In contrast, phosphorylation of full-length EPLIN and the N-terminal region of EPLIN by ERK did not significantly reduce their affinity for F-actin in a similar in vitro actin cosedimentation assay (data not shown).

To test the effect of ERK phosphorylation of EPLIN on its affinity for actin in vivo, Myc-tagged full-length EPLIN or the

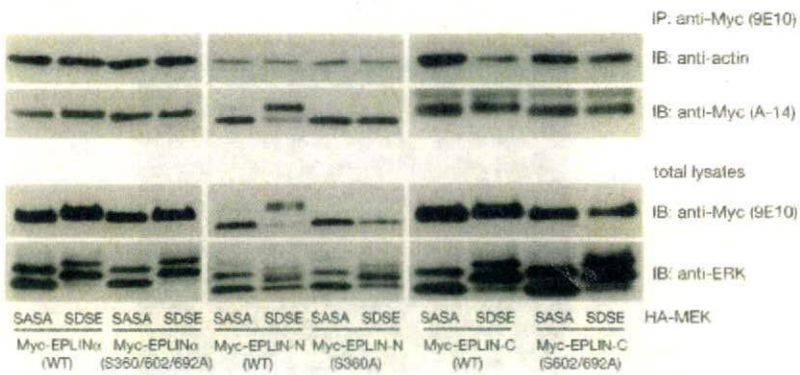

FIG. 4. Phosphorylation of the C-terminal region of EPLIN by ERK reduces its affinity for actin in vivo. 293T cells were cotransfected with Myc-EPLINα, Myc–EPLIN-N, Myc–EPLIN-C, or their Ala substitutes and dominant-negative (SASA) or constitutively active (SDSE) HA-MEK as indicated. The lysates were immunoprecipitated with an anti-Myc (9E10) antibody, followed by immunoblot analysis with antiactin and anti-Myc (A-14) antibodies (upper panels). The total lysates were immunoblotted with anti-Myc (9E10) and anti-ERK antibodies (lower panels).

N-terminal or C-terminal region of EPLIN was coexpressed with constitutively active (SDSE) or dominant-negative (SASA) HA-tagged MEK in 293T cells. Myc-EPLIN was immunoprecipitated with anti-Myc antibody, and immunoprecipitates were subjected to immunoblotting with anti-actin (Fig. 4). The coexpression of MEK-SDSE markedly decreased the binding of EPLIN-C to actin compared to coexpression of MEK-SASA, while the binding of EPLIN-C(S602/692A) did not change upon ERK activation (Fig. 4, right panels). Full-length Myc-EPLINα and Myc–EPLIN-N did not show such a reduction (Fig. 4, left and middle panels). EPLIN may homodimerize through a LIM domain and bind to the side of an actin filament through two actin-binding domains (23). Therefore, it may be reasonable that a reduction in the actin-binding activity of the C-terminal region does not necessarily result in a significant decrease in that of full-length EPLIN (see Fig. 9F).

Stimulation with PDGF induces relocalization of EPLIN to peripheral and dorsal ruffles. To examine whether phosphorylation by ERK regulates EPLIN function in living cells, we first investigated the subcellular localization of EPLIN during ERK activation. Serum-starved NIH 3T3 cells were stimulated with PDGF and then immunostained with anti-EPLIN (Fig. 5A). EPLIN colocalized with actin stress fibers in quiescent cells (Fig. 5A, left panels). PDGF stimulation induced disassembly of stress fibers and formation of peripheral and dorsal ruffles, where EPLIN was relocalized (Fig. 5A, middle panels). When cells were treated with PDGF in the presence of U0126, stress fiber disassembly was partially inhibited, and a fraction of EPLIN localized on the remaining stress fibers (Fig. 5A, right panels). Similar results were obtained with primary osteoblasts (see Fig. 10B).

Stimulation with PDGF induces phosphorylation of Ser360 and Ser602 at peripheral and dorsal ruffles. We then examined the localization of phosphorylated EPLIN in PDGF-stimulated NIH 3T3 cells by indirect immunofluorescence microscopy using anti-pS360 and anti-pS602 antibodies (Fig. 5B and C; the anti-pS692 antibody did not show specific staining). In quiescent cells, phosphorylation of Ser360 was hardly detected. When cells were stimulated with PDGF, Ser360-phosphorylated EPLIN appeared first in peripheral and dorsal ruffles and gradually increased with time (Fig. 5B), consistent with the results of immunoblot analysis (Fig. 2D). U0126 pretreatment or siRNA-mediated depletion of ERK2 or ERK1 plus ERK2 completely abolished the staining by the anti-Ser360 antibody (Fig. 5B and 6B).

Immunostaining with the anti-pS602 antibody revealed that phosphorylation of EPLIN at Ser602 proceeded earlier than that at Ser360 (Fig. 5C). After 5 min of stimulation with PDGF, phosphorylation signals clearly appeared in dorsal ruffles (Fig. 5C, arrowheads). The time course of anti-pS602 staining intensity also correlated well with the results of immunoblot analysis. Phosphorylated ERK (p-ERK) was observed throughout the cell body after 5 min, translocated into the nucleus after 30 min, and returned to the cytoplasm after 120 min (Fig. 5C). These staining patterns with anti-pS602 and anti-p-ERK antibodies were abolished by U0126 pretreatment or siRNA-mediated depletion of ERK2 or ERK1 plus ERK2 (Fig. 5C and 6B and C). Nuclear staining with the anti-pS602 antibody was observed in quiescent cells and in cells pretreated with U0126, suggesting that it may be nonspecific staining.

Ser360- and Ser602-phosphorylated EPLIN localizes to the leading edge of migrating cells. The localization of phosphorylated EPLIN at membrane ruffles prompted us to test whether the phosphorylation of EPLIN occurs during cell migration. Wound healing of fibroblasts causes a rapid and transient activation of ERK at the leading edge, which can be inhibited by U0126 (21, 26). Six hours after wounding of a confluent monolayer of NIH 3T3 cells, cells were immunostained with the anti-pS360 or anti-pS602 antibody (Fig. 7). Both phosphorylated Ser360 and Ser602 were evident in cells at the leading edge. As expected, pretreatment with U0126 completely abolished these staining patterns. These results indicate that EPLIN is phosphorylated by ERK at the leading edge of migrating fibroblasts.

Phosphorylation of EPLIN by ERK is required for PDGF-induced stress fiber disassembly and membrane ruffling. To examine whether the phosphorylation of EPLIN by ERK is involved in membrane ruffling, we constructed EGFP-fused full-length EPLINα (EPLINα-EGFP) and a nonphosphorylatable mutant EPLINα protein [EPLINα(S360/602/692A)-EGFP] in which three major phosphorylation sites were re-

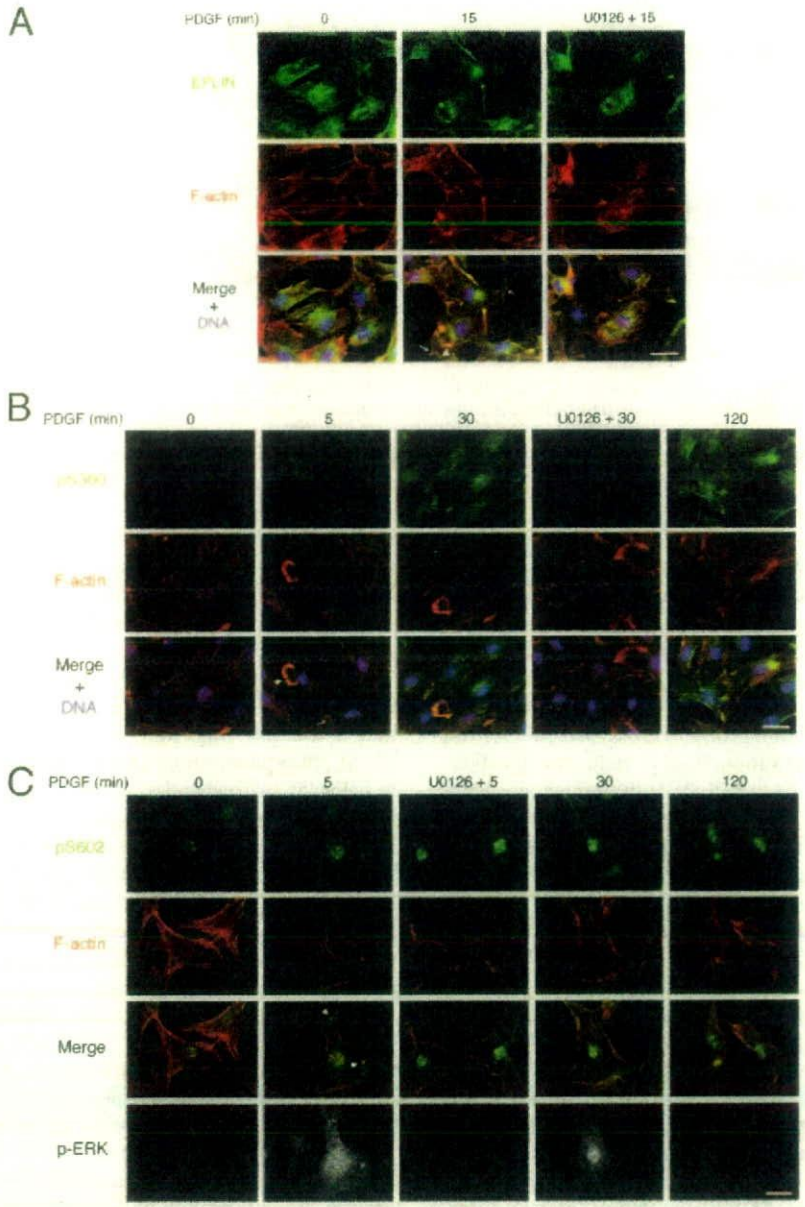

FIG. 5. Stimulation with PDGF induces localization of phosphorylated EPLIN to peripheral and dorsal ruffles. Serum-starved NIH 3T3 cells were stimulated with 50 ng/ml PDGF for the indicated times in the presence or absence of a 30-min pretreatment with U0126. (A) Cells were fixed and stained with the anti-EPLIN antibody (green), rhodamine-phalloidin (red), and DAPI (4′,6′-diamidino-2-phenylindole) (blue). (B) Cells were fixed and stained with the anti-pS360 antibody (green), rhodamine-phalloidin (red), and DAPI (blue). (C) Cells were fixed and stained with the anti-pS602 antibody (green), Alexa Fluor 647-phalloidin (red), and anti-p-ERK antibody (gray). Note that Ser602-phosphorylated EPLIN preferentially localizes to membrane ruffles rather than stress fibers. The arrows and arrowheads indicate peripheral and dorsal ruffles, respectively. Bars, 30 μm.

placed with Ala. Expression of both types of EPLIN increased the number and size of actin stress fibers in quiescent NIH 3T3 cells (Fig. 8A, left panels), as reported previously for MCF-7 cells (23). After stimulation with PDGF, EPLINα-EGFP-expressing cells lost their stress fibers and formed prominent lamellipodia/membrane ruffles, but EPLINα(S360/602/692A)-EGFP-expressing cells still retained stress fibers and formed fewer membrane ruffles (Fig. 8A, right panels; see Videos S1 and S2 in the supplemental material).

EGPF-positive cells were categorized into four classes according to their degree of ruffling (Fig. 8B). Among quiescent cells, most wild type- and Ala mutant-transfected cells were classified as type I (without ruffles). When cells were stimulated with PDGF for 5 min, EPLINα-EGFP-expressing cells were mostly classified into types III and IV, with marked lamellipodia/membrane ruffles, but in EPLINα(S360/602/692A)-EGFP-expressing cells ruffle formation was significantly impaired. These data suggest that phosphorylation of EPLIN by

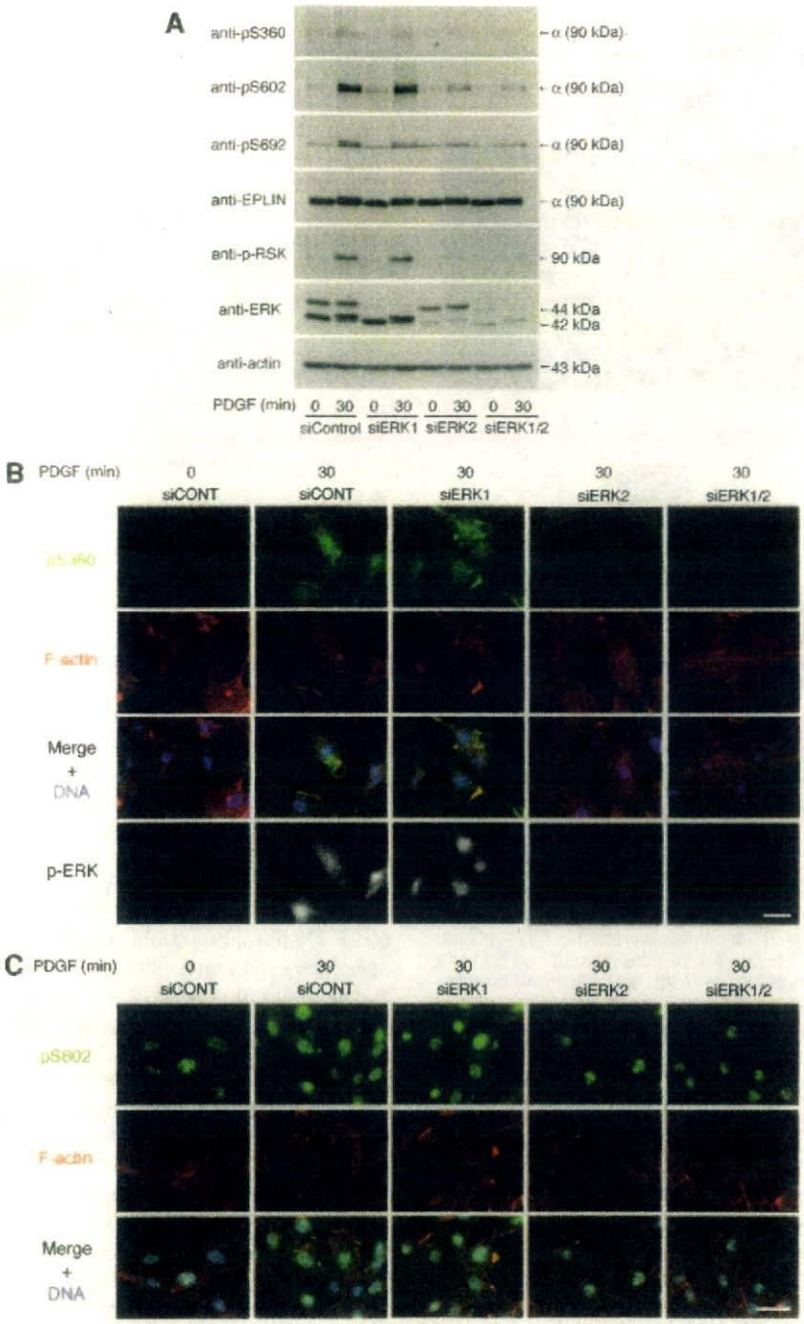

FIG. 6. PDGF-induced phosphorylation of EPLIN is inhibited by siRNA-mediated depletion of ERK2 or ERK1 plus ERK2. NIH 3T3 cells were transfected with siRNA for control, ERK1, ERK2, or ERK1 plus ERK2, incubated for 48 h, serum starved, and then stimulated with 50 ng/ml PDGF for 0 or 30 min. (A) The lysates were immunoblotted with the indicated antibodies. (B) Cells were fixed and quadruply stained with the anti-pS360 antibody (green), Alexa Fluor 647-phalloidin (red), DAPI (blue), and anti-p-ERK antibody (gray). (C) Cells were fixed and triply stained with the anti-pS602 antibody (green), rhodamine-phalloidin (red), and DAPI (blue). Bars, 30 μm.

ERK is involved in PDGF-induced lamellipodium/membrane ruffle formation.

Phosphorylation of EPLIN by ERK is required for cell migration. Dynamic phosphorylation and dephosphorylation of cytoskeletal proteins are essential for effective cell motility. To evaluate the potential role of EPLIN phosphorylation in cell migration, wound-healing assays were performed using EPLINα-EGFP- and EPLINα(S360/602/692A)-EGFP-transfected NIH 3T3 cells. The proportion of EGFP-positive cells at the wound edge was assessed over an 8-h time period. The ratio of EPLINα-EGFP expression at the wound edge (approximately 20%) did not change during

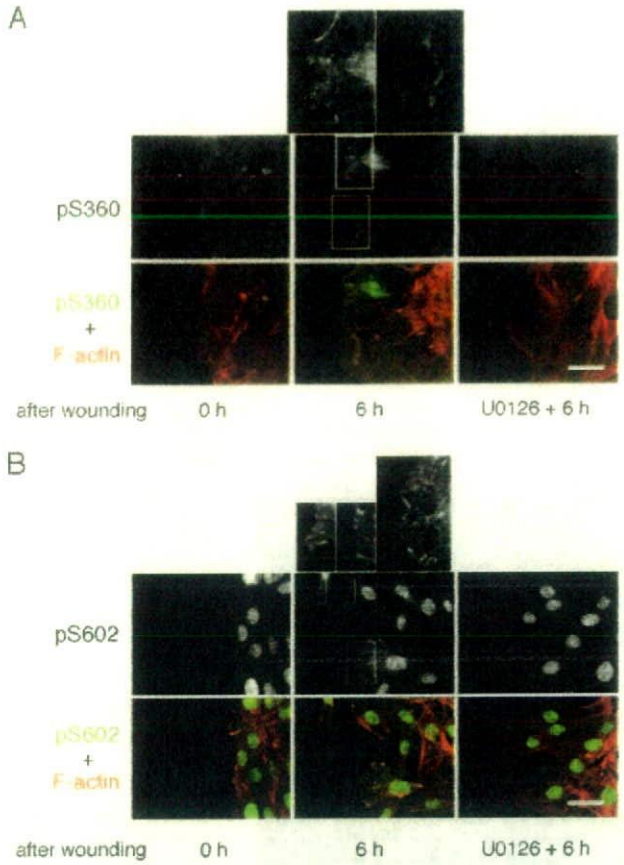

FIG. 7. EPLIN is phosphorylated at the leading edge of migrating fibroblasts during recovery from a wound. A confluent monolayer of NIH 3T3 cells was "wounded" by being scraped with a plastic pipette tip and then cultured for 0 or 6 h in the presence or absence of a 30-min pretreatment with U0126. Cells were fixed and doubly stained with the anti-pS360 (A) or anti-pS602 (B) antibody and rhodamine-phalloidin (red). The wound site is at the left of each panel. Bars, 50 μm.

this period, indicating that EPLINα-EGFP-expressing cells and surrounding untransfected cells migrated at similar velocities (Fig. 9A; see Video S3 in the supplemental material). In contrast, the EPLINα(S360/602/692A)-EGFP-expressing cells showed a marked decrease in motility and gradually fell behind the wound edge during recovery (Fig. 9A; see Video S4 in the supplemental material). These results indicate that EPLIN phosphorylation by ERK is required for cell migration during wound healing.

The roles of EPLIN phosphorylation by ERK in cell motility were evaluated in another experiment, a modified Boyden chamber assay. The addition of PDGF to the lower chamber induced migration of NIH 3T3 cells expressing EGFP or EPLINα-EGFP, and pretreatment with U0126 inhibited PDGF-induced migration of these cells (Fig. 9B). In contrast, expression of EPLINα(S360/602/692A)-EGFP significantly inhibited PDGF-induced migration compared with expression of EGFP or EPLINα-EGFP (Fig. 9B). Similar results were obtained with primary osteoblasts (Fig. 10C). These results suggest that EPLIN phosphorylation by ERK is also required for PDGF-induced cell migration.

To further investigate the functions of EPLIN in cell motility, siRNA-mediated depletion of EPLIN and rescue assays were performed. We prepared RNAi-refractory versions of EPLIN proteins [EPLINαr-EGFP and EPLINαr(S360/602/692A)-EGFP] harboring silent mutations (Fig. 9C). EPLIN depletion significantly enhanced the ability of NIH 3T3 cells to migrate in both the wound-healing assay and the modified Boyden chamber assay (Fig. 9D and E), suggesting that EPLIN functions to negatively influence cell motility. While expression of EPLINαr-EGFP efficiently restored the enhanced migratory activity to the level seen with control siRNA treatment, EPLINαr(S360/602/692A)-EGFP-expressing cells showed a significant decrease in motility compared with control siRNA-treated or EPLINαr-EGFP-expressing cells (Fig. 9D and E). We also confirmed these findings by performing modified Boyden chamber assays with primary osteoblasts (Fig. 10D). Taken together, these results indicate that EPLIN phosphorylation by ERK is required for cell migration.

DISCUSSION

In the present study, we have characterized an F-actin cross-linking protein, EPLIN, as a novel ERK MAPK substrate. First, ERK phosphorylates EPLIN on Ser360, Ser602, and Ser692 in vitro and in living cells. Second, ERK phosphorylation of EPLIN decreases the affinity of its C-terminal region for actin filaments. Third, EPLIN localizes to actin stress fibers in quiescent cells, and stimulation with PDGF induces relocalization of EPLIN to lamellipodia/membrane ruffles. Fourth, phosphorylated EPLIN localizes to membrane ruffles both upon PDGF stimulation and during wound healing. Fifth, a non-ERK-phosphorylatable mutant of EPLIN inhibits PDGF-dependent actin stress fiber disassembly, membrane ruffling, and cell migration, while RNAi-mediated silencing of EPLIN enhances cell motility. ERK thus controls actin organization and cell motility by phosphorylating EPLIN.

ERK phosphorylation sites within EPLIN were identified by site-directed mutagenesis. We determined that the Ser360, Ser602, and Ser692 residues of EPLIN are the major phosphorylation sites for ERK. These phosphorylation sites were confirmed by LC-MS/MS analysis of in vitro-phosphorylated EPLIN (see Fig. S2A, C, and D in the supplemental material). Immunoblot analysis using phospho-specific antibodies revealed that these three sites are indeed phosphorylated by ERK in intact cells (Fig. 2D and 10A). Although recent phosphoproteomic studies detected intracellular phosphorylation of mouse EPLIN at Ser360 (43) and of human EPLIN at Ser604 and Ser698 (corresponding to Ser602 and Ser692 of mouse EPLIN) (27, 28), spatiotemporal changes had not been reported. Interestingly, PDGF-induced phosphorylation of Ser360 occurred rather slowly compared to the rapid phosphorylation of Ser602, Ser692, and ERK (Fig. 2D). This raises the possibility that cellular phosphatase activity toward Ser360 is high in the early phase or that ERK indirectly phosphorylates Ser360 through a downstream kinase.

EPLIN contains two actin-binding sites, in the N- and C-terminal halves, and a LIM domain between these sites may allow EPLIN to homodimerize. EPLIN therefore cross-links

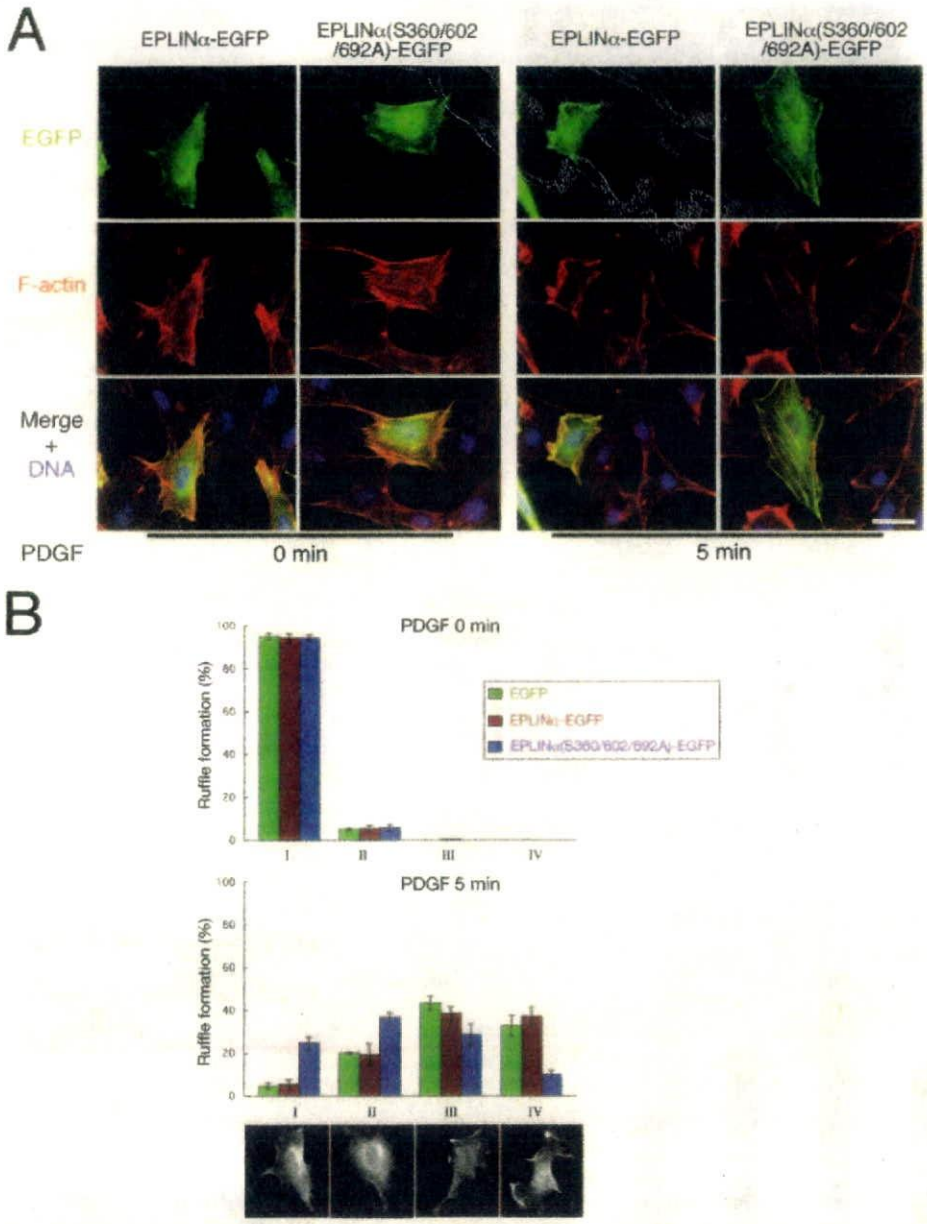

FIG. 8. Phosphorylation of EPLIN is required for PDGF-induced stress fiber disassembly and membrane ruffling. (A) NIH 3T3 cells transfected with EPLINα-EGFP or EPLINα(S360/602/692A)-EGFP were stimulated with 50 ng/ml PDGF for 0 or 5 min. Cells were fixed and stained with rhodamine-phalloidin and DAPI to detect F-actin (red) and DNA (blue), respectively. Bar, 30 μm. (B) NIH 3T3 cells transfected with EGFP, EPLINα-EGFP, or EPLINα(S360/602/692A)-EGFP were stimulated with 50 ng/ml PDGF for 0 or 5 min. The degree of ruffling was categorized into four classes, as exemplified in the bottom panels. At least 100 cells were counted per sample, and values are means ± standard deviations (SD) for three independent experiments.

and bundles actin filaments, but the two actin-binding domains may have different functions in the cell (23). In cosedimentation assays with F-actin, we found that the C-terminal half of EPLIN, but neither full-length EPLIN nor the N-terminal half of EPLIN, reduces its association with F-actin upon ERK-mediated phosphorylation. This observation was confirmed by an in vivo experiment showing that the amount of actin coimmunoprecipitated with the C-terminal half but neither full-length EPLIN nor the N-terminal half of EPLIN was reduced by activation of ERK. Since EPLIN is supposed to bind to the side of an actin filament through two actin-binding domains (23), it may be reasonable that a reduction in the actin-binding activity of the C-terminal region does not necessarily lead to a significant decrease in that of full-length EPLIN (Fig. 9F).

The phosphorylation-dependent reduction of the affinity of the C-terminal region for F-actin may affect the actin-bundling activity of EPLIN to facilitate dynamic remodeling of actin filament networks. Thus, we investigated the effects of EPLIN

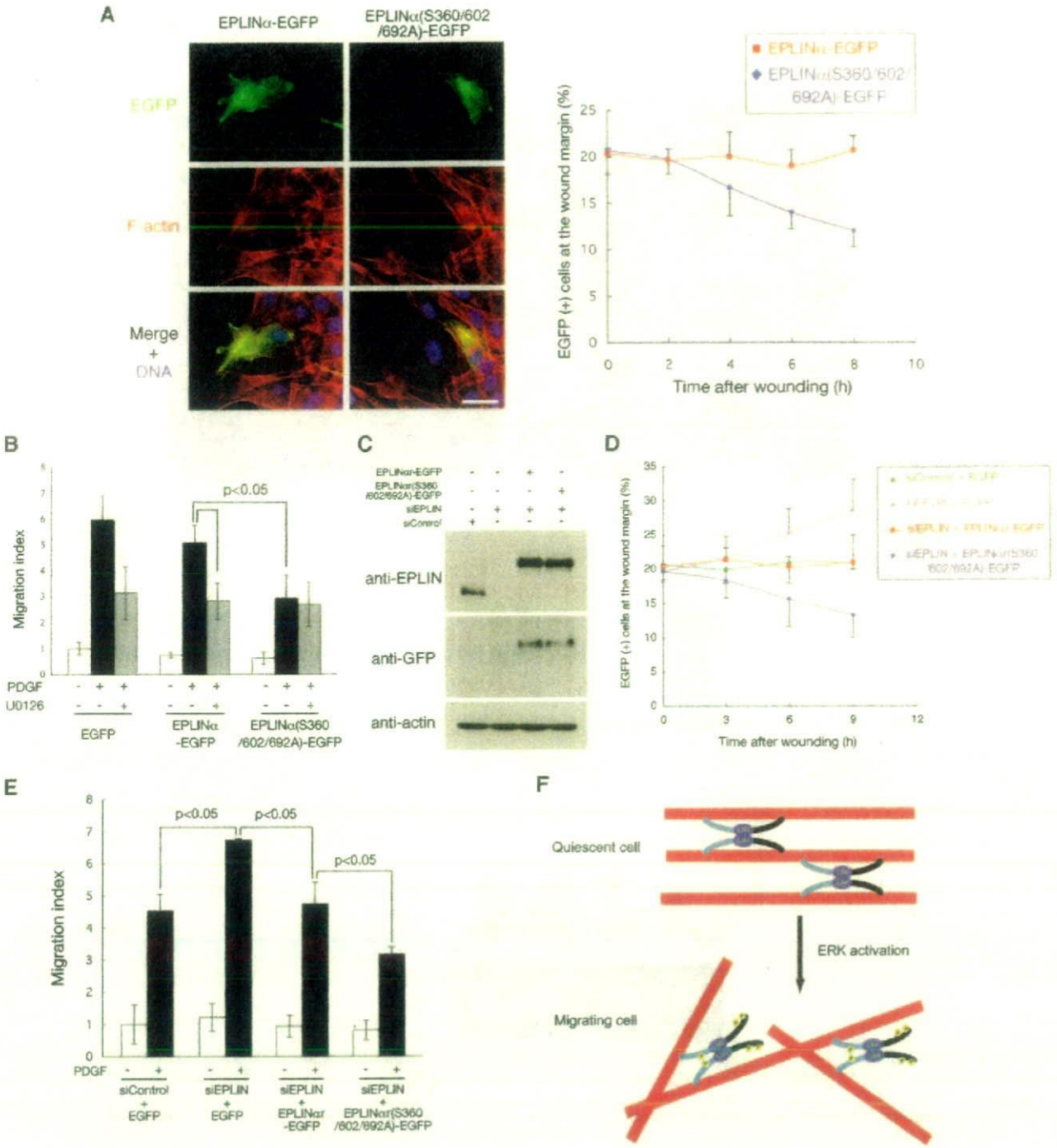

FIG. 9. Phosphorylation of EPLIN is required for cell migration. (A) Six hours after wounding of a confluent monolayer of NIH 3T3 cells transfected with EPLINα-EGFP or EPLINα(S360/602/692A)-EGFP, cells were fixed and stained with rhodamine-phalloidin and DAPI to detect F-actin (red) and DNA (blue), respectively (left panels; both EGFP-positive cells were located at the margin immediately after being wounded). The wound site is at the left of each panel. Bar, 50 μm. At the indicated times after wounding, the proportion of EGFP-positive cells at the wound margin was assessed (right panel). (B) NIH 3T3 cells were transfected with EGFP, EPLINα-EGFP, or EPLINα(S360/602/692A)-EGFP. After 24 h, a modified Boyden chamber assay was performed in the absence or presence of 30 ng/ml PDGF in the lower chamber. PDGF-induced migration was also observed in the presence of 20 μM U0126 in both the upper and lower chambers. (C) NIH 3T3 cells were transfected with control siRNA or EPLIN siRNA, incubated for 24 h, and then transfected with EGFP, RNAi-refractory EPLINαr-EGFP, or EPLINαr(S360/602/692A)-EGFP. After 24 h of incubation, the lysates were immunoblotted with the indicated antibodies. (D) At the indicated times after being wounded, a confluent monolayer of NIH 3T3 cells that had been transfected simultaneously as indicated were fixed and stained as described for panel A, and the proportion of EGFP-positive cells at the wound margin was assessed. (E) NIH 3T3 cells were sequentially transfected as described for panel C and then subjected to a modified Boyden chamber assay in the absence or presence of 30 ng/ml PDGF in the lower chamber. For panels A, B, D, and E, at least 100 cells were counted per sample, and values are means ± SD for three independent experiments. (F) Schematic representation of the proposed mechanism by which ERK-mediated phosphorylation of the C-terminal region of EPLIN leads to reorganization of actin filaments.

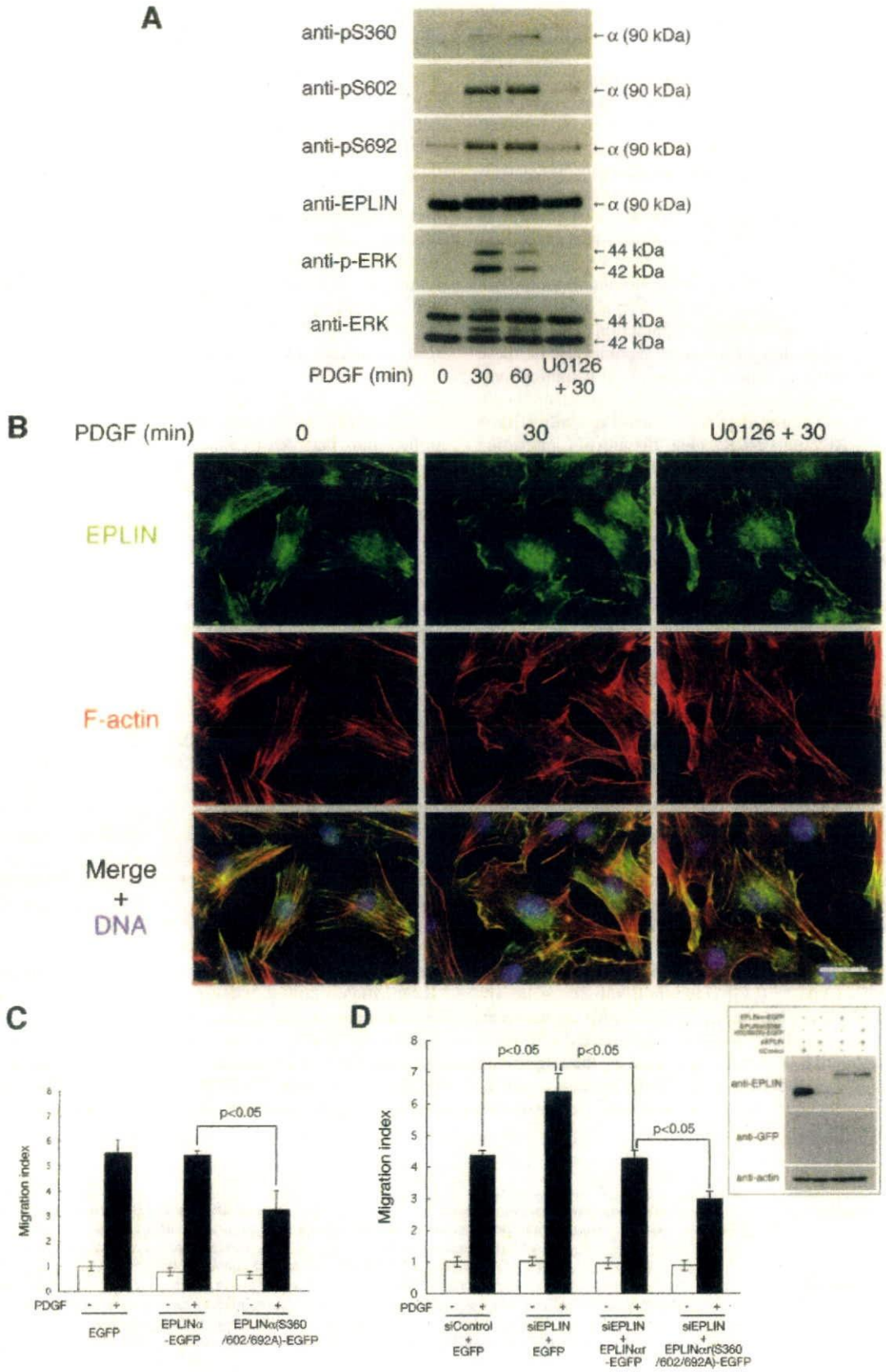

phosphorylation on its localization, actin dynamics, and cell motility. It has been reported that endogenous EPLIN is distributed predominantly along actin stress fibers in U2OS cells (35). Consistent with this finding, immunostaining showed that EPLIN colocalized with stress fibers in quiescent NIH 3T3 cells (Fig. 5A) and primary osteoblasts (Fig. 10B). Stimulation with PDGF induced stress fiber disassembly and relocalization of EPLIN to membrane ruffles within 15 to 30 min. When cells were treated with PDGF in the presence of U0126, stress fiber disassembly was partly inhibited by blocking the ERK pathway (29), and a fraction of EPLIN remained localized on the resultant stress fibers.

We further demonstrated by indirect immunofluorescence microscopy that both Ser360 and Ser602 are phosphorylated in specific subcellular areas by PDGF stimulation or during cell migration, suggesting the physiological significance of these phosphorylation sites in cellular processes. Both staining patterns were not detectable when the cells were pretreated with U0126 (Fig. 5B and C and Fig. 7) or transfected with siRNA for ERK2 or ERK1 plus ERK2 (Fig. 6B and C), indicating ERK-dependent phosphorylation. PDGF treatment induced the phosphorylation of EPLIN at peripheral and dorsal ruffles. In migrating NIH 3T3 fibroblasts, phosphorylated EPLIN preferentially localized to the leading edge, which is consistent with previous observations that activated ERK is also localized at the leading edge during migration of rat embryo fibroblasts and 3Y1 cells (21, 26). These findings support the possible involvement of EPLIN phosphorylation by ERK in actin reorganization and cell migration (see below).

To clarify the effects of EPLIN phosphorylation on actin organization and cell motility, we used wild-type EPLIN and a non-ERK-phosphorylatable mutant EPLINα fused to EGFP. The nonphosphorylatable mutant inhibited both cellular processes. The precise molecular mechanism by which ERK promotes ruffle formation and cell migration via phosphorylating EPLIN remains unclear. Since the mutant contains substitutions in both the N- and C-terminal regions, there remained the possibility that the reduction of the affinity of the C-terminal region for F-actin may not participate in this mechanism. However, in a modified Boyden chamber assay, two substitutions in the C-terminal region [EPLINα(S602/692A)-EGFP migration index, 3.53 ± 0.46] showed a similar inhibitory effect to that by three substitutions [EPLINα(S360/602/692A)-EGFP migration index, 3.03 ± 0.35] compared with the wild type (EPLINα-EGFP migration index, 5.17 ± 0.47) or a protein with one substitution in the N-terminal region [EPLINα(S360A)-EGFP migration index, 4.67 ± 0.52], indicating the importance of a phosphorylation-dependent reduction in the C-terminal binding activity. Phosphorylation of Ser360 in the N-terminal region causes an electrophoretic mobility shift (see Fig. S1 in the supplemental material), suggesting conformational and functional changes that should be addressed in future studies. Since nonphosphorylated EPLIN dimers can form thick actin bundles through the N- and C-terminal actin-binding sites, EPLIN in quiescent cells may stabilize stress fibers and inhibit cell migration (Fig. 9F, upper panel). Phosphorylated EPLIN dimers can cross-link actin filaments through only the N-terminal actin-binding sites, and thereby EPLIN in migrating cells may form a dynamic actin meshwork in membrane ruffles (Fig. 9F, lower panel). Taken together, the data show that PDGF stimulation activates ERK, which phosphorylates EPLIN to reduce the affinity of its C-terminal region for actin filaments, and then phosphorylated EPLIN causes destabilization of stress fibers and reorganization of the actin cytoskeleton to form membrane ruffles and to enhance cell migration.

ERK is known to regulate actin organization and cell motility by phosphorylating a number of proteins, including MLCK, FAK, paxillin, actopaxin, and vinexin. We demonstrate in this study that EPLIN is also a mediator of ERK-regulated cytoskeletal dynamics. Because the expression of phosphomimetic mutants of EPLIN had weak effects on these processes (data not shown), many actin-binding proteins phosphorylated by ERK are likely to act in concert to regulate actin dynamics. Furthermore, various extracellular stimuli induce actin reorganization and cell migration through other ERK-independent pathways. For example, it was recently reported that Akt regulates these processes via phosphorylation of girdin, an F-actin cross-linking protein (7). Other actin cross-linking proteins, such as fascin (42, 45) and L-plastin (15), were also shown to be regulated by phosphorylation to control actin cytoskeletal assembly and cell motility.

It has been reported that EPLIN is down-regulated or lost in a number of oral, prostate, and breast cancer cell lines (3, 22). Since siRNA-mediated depletion of EPLIN enhanced cell motility during wound healing and in PDGF-induced cell migration, the down-regulation of EPLIN expression might be relevant to migration and invasion of these cancer cells. Previously, it was reported that ectopic expression of EPLIN can suppress anchorage-independent growth of NIH 3T3 cells transformed by Cdc42V12 or EWS/Fli-1 but not by RasV12 (35). This can now be explained by actin reorganization and enhanced cell motility through the Ras-Raf-MEK-ERK-EPLIN pathway. Ras-mediated phosphorylation of EPLIN may be involved in the invasion of tumor cells with Ras mutations. EPLIN is highly conserved from zebra fish to humans and contains multiple Ser/Thr-Pro motifs that can potentially be phosphorylated by ERK. The ERK-EPLIN pathway may play important roles in diverse physiological processes in vertebrates.

FIG. 10. Phosphorylation of EPLIN by ERK is required for cell migration in primary calvarial osteoblasts. (A and B) Serum-starved osteoblasts were treated with 50 ng/ml PDGF for the indicated times in the presence or absence of a 30-min pretreatment with U0126. (A) The lysates were immunoblotted with the indicated antibodies. (B) Cells were fixed and stained with the anti-EPLIN antibody (green), rhodamine-phalloidin (red), and DAPI (blue). Bar, 30 μm. (C) Osteoblasts were transfected with EGFP, EPLINα-EGFP, or EPLINα(S360/602/692A)-EGFP. After 24 h, a modified Boyden chamber assay was performed in the absence or presence of 30 ng/ml PDGF in the lower chamber. (D) Osteoblasts sequentially transfected with control siRNA or EPLIN siRNA and EGFP, EPLINαr-EGFP, or EPLINαr(S360/602/692A)-EGFP were subjected to a modified Boyden chamber assay in the absence or presence of 30 ng/ml PDGF in the lower chamber. The inset shows the depletion of endogenous EPLINα by siRNA and the rescue by RNAi-refractory EPLINαr-EGFP or EPLINαr(S360/602/692A)-EGFP. For panels C and D, at least 100 cells were counted per sample, and values are means ± SD for three independent experiments.

ACKNOWLEDGMENTS

We thank Michimoto Kobayashi for his help during the initial stages of this work, Yutaka Harita for help with rabbit immunization, Makoto Watanabe for help with isolating primary calvarial osteoblasts, Hiroyuki Fukuda for LC-MS/MS analysis, Miho Ohsugi and Noriko Tokai-Nishizumi for help with time-lapse video microscopy, Masanori Mishima and Max Douglas for critical readings of the manuscript, and Shiro Suetsugu and Eisuke Nishida for helpful discussions and advice. We also thank Martin McMahon for kindly providing ΔB-Raf:ER cells.

This work was supported in part by grants-in-aid for scientific research from the Japan Society for the Promotion of Science (to H.K.) and the Encouraging Development Strategic Research Centers Program, Special Coordination Funds for Promoting Science and Technology, the Ministry of Education, Culture, Sports, Science, and Technology (to S.H.). This work was also supported by grants from the Nakajima Foundation (to H.K.) and the Novartis Foundation (Japan) for the Promotion of Science (to S.H.). This work was developed and coordinated under the framework of the program for the International Research and Educational Institute for Integrated Medical Sciences (IREIIMS).

REFERENCES

1. **Adams, J. C.** 2004. Roles of fascin in cell adhesion and motility. Curr. Opin. Cell Biol. **16**:590–596.
2. **Bartles, J. R.** 2000. Parallel actin bundles and their multiple actin-bundling proteins. Curr. Opin. Cell Biol. **12**:72–78.
3. **Chang, D. D., N. H. Park, C. T. Denny, S. F. Nelson, and M. Pe.** 1998. Characterization of transformation related genes in oral cancer cells. Oncogene **16**:1921–1930.
4. **Chang, L., and M. Karin.** 2001. Mammalian MAP kinase signalling cascades. Nature **410**:37–40.
5. **Clarke, D. M., M. C. Brown, D. P. LaLonde, and C. E. Turner.** 2004. Phosphorylation of actopaxin regulates cell spreading and migration. J. Cell Biol. **166**:901–912.
6. **Cox, B. D., M. Natarajan, M. R. Stettner, and C. L. Gladson.** 2006. New concepts regarding focal adhesion kinase promotion of cell migration and proliferation. J. Cell Biochem. **99**:35–52.
7. **Enomoto, A., H. Murakami, N. Asai, N. Morone, T. Watanabe, K. Kawai, Y. Murakumo, J. Usukura, K. Kaibuchi, and M. Takahashi.** 2005. Akt/PKB regulates actin organization and cell motility via Girdin/APE. Dev. Cell **9**:389–402.
8. **Etienne-Manneville, S., and A. Hall.** 2002. Rho GTPases in cell biology. Nature **420**:629–635.
9. **Fincham, V. J., M. James, M. C. Frame, and S. J. Winder.** 2000. Active ERK/MAP kinase is targeted to newly forming cell-matrix adhesions by integrin engagement and v-Src. EMBO J. **19**:2911–2923.
10. **Glading, A., R. J. Bodnar, I. J. Reynolds, H. Shiraha, L. Satish, D. A. Potter, H. C. Blair, and A. Wells.** 2004. Epidermal growth factor activates m-calpain (calpain II), at least in part, by extracellular signal-regulated kinase-mediated phosphorylation. Mol. Cell. Biol. **24**:2499–2512.
11. **Gonzalez, F. A., D. L. Raden, and R. J. Davis.** 1991. Identification of substrate recognition determinants for human Erk1 and Erk2 protein kinases. J. Biol. Chem. **266**:22159–22163.
12. **Hazzalin, C. A., and L. C. Mahadevan.** 2002. MAPK-regulated transcription: a continuously variable gene switch? Nat. Rev. Mol. Cell. Biol. **3**:30–40.
13. **Huang, C., K. Jacobson, and M. D. Schaller.** 2004. MAP kinases and cell migration. J. Cell Sci. **117**:4619–4628.
14. **Hunger-Glaser, I., E. P. Salazar, J. Sinnett-Smith, and E. Rozengurt.** 2003. Bombesin, lysophosphatidic acid, and epidermal growth factor rapidly stimulate focal adhesion kinase phosphorylation at Ser-910: requirement for ERK activation. J. Biol. Chem. **278**:22631–22643.
15. **Janji, B., A. Giganti, V. De Corte, M. Catillon, E. Bruyneel, D. Lentz, J. Plastino, J. Gettemans, and E. Friederich.** 2006. Phosphorylation on Ser5 increases the F-actin-binding activity of L-plastin and promotes its targeting to sites of actin assembly in cells. J. Cell Sci. **119**:1947–1960.
16. **Klemke, R. L., S. Cai, A. L. Giannini, P. J. Gallagher, P. de Lanerolle, and D. A. Cheresh.** 1997. Regulation of cell motility by mitogen activated protein kinase. J. Cell Biol. **137**:481–492.
17. **Kondoh, K., S. Torii, and E. Nishida.** 2005. Control of MAP kinase signaling to the nucleus. Chromosoma **114**:86–91.
18. **Lewis, T. S., P. S. Shapiro, and N. G. Ahn.** 1998. Signal transduction through MAP kinase cascades. Adv. Cancer Res. **74**:49–139.
19. **Liu, Z. X., C. F. Yu, C. Nickel, S. Thomas, and L. G. Cantley.** 2002. Hepatocyte growth factor induces ERK-dependent paxillin phosphorylation and regulates paxillin-focal adhesion kinase association. J. Biol. Chem. **277**:10452–10458.
20. **Machida, M., H. Kosako, K. Shirakabe, M. Kobayashi, M. Ushiyama, J. Inagawa, J. Hirano, T. Nakano, Y. Bando, E. Nishida, and S. Hattori.** 2007. Purification of phosphoproteins by immobilized metal affinity chromatography and its application to phosphoproteome analysis. FEBS J. **274**:1576–1587.
21. **Matsubayashi, Y., M. Ebisuya, S. Honjoh, and E. Nishida.** 2004. ERK activation propagates in epithelial cell sheets and regulates their migration during wound healing. Curr. Biol. **14**:731–735.
22. **Maul, R. S., and D. D. Chang.** 1999. EPLIN, epithelial protein lost in neoplasm. Oncogene **18**:7838–7841.
23. **Maul, R. S., Y. Song, K. J. Amann, S. C. Gerbin, T. D. Pollard, and D. D. Chang.** 2003. EPLIN regulates actin dynamics by cross-linking and stabilizing filaments. J. Cell Biol. **160**:399–407.
24. **Mitsushima, M., A. Suwa, T. Amachi, K. Ueda, and N. Kioka.** 2004. Extracellular signal-regulated kinase activated by epidermal growth factor and cell adhesion interacts with and phosphorylates vinexin. J. Biol. Chem. **279**:34570–34577.
25. **Nguyen, D. H., A. D. Catling, D. J. Webb, M. Sankovic, L. A. Walker, A. V. Somlyo, M. J. Weber, and S. L. Gonias.** 1999. Myosin light chain kinase functions downstream of Ras/ERK to promote migration of urokinase-type plasminogen activator-stimulated cells in an integrin-selective manner. J. Cell Biol. **146**:149–164.
26. **Nobes, C. D., and A. Hall.** 1999. Rho GTPases control polarity, protrusion, and adhesion during cell movement. J. Cell Biol. **144**:1235–1244.
27. **Nousiainen, M., H. H. W. Silljé, G. Sauer, E. A. Nigg, and R. Körner.** 2006. Phosphoproteome analysis of the human mitotic spindle. Proc. Natl. Acad. Sci. USA **103**:5391–5396.
28. **Olsen, J. V., B. Blagoev, F. Gnad, B. Macek, C. Kumar, P. Mortensen, and M. Mann.** 2006. Global, in vivo, and site-specific phosphorylation dynamics in signaling networks. Cell **127**:635–648.
29. **Orr, A. W., M. A. Pallero, and J. E. Murphy-Ullrich.** 2002. Thrombospondin stimulates focal adhesion disassembly through Gi- and phosphoinositide 3-kinase-dependent ERK activation. J. Biol. Chem. **277**:20453–20460.
30. **Pearson, G., F. Robinson, T. B. Gibson, B. E. Xu, M. Karandikar, K. Berman, and M. H. Cobb.** 2001. Mitogen-activated protein (MAP) kinase pathways: regulation and physiological functions. Endocr. Rev. **22**:153–183.
31. **Pollard, T. D., and G. G. Borisy.** 2003. Cellular motility driven by assembly and disassembly of actin filaments. Cell **112**:453–465.
32. **Pritchard, C. A., M. L. Samuels, E. Bosch, and M. McMahon.** 1995. Conditionally oncogenic forms of the A-Raf and B-Raf protein kinases display different biological and biochemical properties in NIH 3T3 cells. Mol. Cell. Biol. **15**:6430–6442.
33. **Revenu, C., R. Athman, S. Robine, and D. Louvard.** 2004. The co-workers of actin filaments: from cell structures to signals. Nat. Rev. Mol. Cell. Biol. **5**:635–646.
34. **Ridley, A. J.** 2001. Rho GTPases and cell migration. J. Cell Sci. **114**:2713–2722.
35. **Song, Y., R. S. Maul, C. S. Gerbin, and D. D. Chang.** 2002. Inhibition of anchorage-independent growth of transformed NIH3T3 cells by epithelial protein lost in neoplasm (EPLIN) requires localization of EPLIN to actin cytoskeleton. Mol. Biol. Cell **13**:1408–1416.
36. **Stambolic, V., and J. R. Woodgett.** 2006. Functional distinctions of protein kinase B/Akt isoforms defined by their influence on cell migration. Trends Cell Biol. **16**:461–466.
37. **Stossel, T. P., J. Condeelis, L. Cooley, J. H. Hartwig, A. Noegel, M. Schleicher, and S. S. Shapiro.** 2001. Filamins as integrators of cell mechanics and signaling. Nat. Rev. Mol. Cell. Biol. **2**:138–145.
38. **Stupack, D. G., S. Y. Cho, and R. L. Klemke.** 2000. Molecular signaling mechanisms of cell migration and invasion. Immunol. Res. **21**:83–88.
39. **Suetsugu, S., and T. Takenawa.** 2007. Stress-associated MAP kinase fills in the map of filamin-mediated neuronal migration. Dev. Cell **12**:3–4.
40. **Tomar, A., Y. Wang, N. Kumar, S. George, B. Ceacareanu, A. Hassid, K. E. Chapman, A. M. Aryal, C. M. Waters, and S. Khurana.** 2004. Regulation of cell motility by tyrosine phosphorylated villin. Mol. Biol. Cell **15**:4807–4817.
41. **Ueda, K., H. Kosako, Y. Fukui, and S. Hattori.** 2004. Proteomic identification of Bcl2-associated athanogene 2 as a novel MAPK-activated protein kinase 2 substrate. J. Biol. Chem. **279**:41815–41821.
42. **Vignjevic, D., S. Kojima, Y. Aratyn, O. Danciu, T. Svitkina, and G. G. Borisy.** 2006. Role of fascin in filopodia protrusion. J. Cell Biol. **174**:863–875.
43. **Villén, J., S. A. Beausoleil, S. A. Gerber, and S. P. Gygi.** 2007. Large-scale phosphorylation analysis of mouse liver. Proc. Natl. Acad. Sci. USA **104**:1488–1493.
44. **Waskiewicz, A. J., and J. A. Cooper.** 1995. Mitogen and stress response pathways: MAP kinase cascades and phosphatase regulation in mammals and yeast. Curr. Opin. Cell Biol. **7**:798–805.
45. **Yamakita, Y., S. Ono, F. Matsumura, and S. Yamashiro.** 1996. Phosphorylation of human fascin inhibits its actin binding and bundling activities. J. Biol. Chem. **271**:12632–12638.
46. **Zhang, Z., S. Y. Lin, B. G. Neel, and B. Haimovich.** 2006. Phosphorylated α-actinin and protein-tyrosine phosphatase 1B coregulate the disassembly of the focal adhesion kinase × Src complex and promote cell migration. J. Biol. Chem. **281**:1746–1754.

Meeting Report on the 13th International Conference on Human Retrovirology: Human T-Cell Leukemia Virus Research 30 Years after Adult T-Cell Leukemia

Masao Matsuoka,[1] Toshiki Watanabe,[2] Mari Kannagi,[3] Charles Bangham,[4] Ralph Grassmann,[5] Susan J. Marriott,[6] Patrick Green,[7] and Kuan-Teh Jeang[8]

[1]Institute for Virus Research, Kyoto University, Kyoto, Japan; [2]Laboratory of Tumor Cell Biology, University of Tokyo and [3]Department of Immunotherapeutics, Tokyo Medical and Dental University, Tokyo, Japan; [4]Department of Immunology, Imperial College Faculty of Medicine, London, United Kingdom; [5]Institute of Clinical and Molecular Virology, University Erlangen-Nuremberg, Erlangen, Germany; [6]Department of Molecular Virology and Microbiology, Baylor College of Medicine, Houston, Texas; [7]Department of Veterinary Biosciences, Ohio State University, Columbus, Ohio; and [8]Laboratory of Molecular Microbiology, National Institute of Allergy and Infectious Diseases, Bethesda, Maryland

Introduction

Thirty years ago, in 1977, a new clinical entity called adult T-cell leukemia (ATL) was described in Japan by Takatsuki and colleagues. Subsequently, Poiesz, Ruscetti, Gallo, and coworkers; and Yoshida, Miyoshi, Hinuma, and colleagues isolated a human retrovirus named human T-cell leukemia virus type-1 (HTLV-1). The history of the discovery of ATL and the isolation of HTLV-1 has been recently reviewed elsewhere (1–3).

From May 22 to 25, 2007, 350 researchers gathered in Hakone, Japan, at the 13th International Conference on Human Retrovirology organized by Toshiki Watanabe (University of Tokyo, Tokyo, Japan) to discuss the latest finding on HTLV-1 pathogenesis. The meeting opened with a keynote presentation by Kuan-Teh Jeang [National Institute of Allergy and Infectious Diseases (NIAID), Bethesda, MD] reviewing cell proliferative changes, genetic damaging events, and check point inactivation in the development of ATL (4). Over the next 4 days, >320 papers were presented. Conference highlights are summarized below.

Epidemiology of HTLV

HTLV infects 10 to 20 million individuals worldwide. Masahiro Satake (Tokyo Red Cross Blood Center, Tokyo, Japan) reported on HTLV-1 positivity rate (0.37%) in Japanese first-time blood donors. HTLV-1 seropositivity in donors was 1.18% in their 30s in 1995 and 1.28% in their 40s in 2005, showing an 8% increase in 10 years. The same trend was found in the donors who were an additional 10 years older. Satake interpreted these figures to reveal the rate of horizontal infection in Japan. How individuals become susceptible to HTLV infection was commented upon by Sabine Plancoulaine [Institut National de la Sante et de la Recherche Medicale (INSERM), Paris, France] using a genome-wide linkage analysis mapping the susceptibility locus in children of African origin for HTLV-1 infection through breast feeding. She found significant linkage between HTLV-1 susceptibility and two chromosomal loci at 2p25 and 6q27.

HTLV-1 infection is also associated with an inflammatory pathology termed HTLV-associated myelopathy (HAM) or tropical spastic paraparesis (TSP). The association of neurologic abnormalities and HTLV-1 infection was discussed by Edward Murphy (University of California San Francisco, San Francisco, CA). In his study (HTLV Outcome Study), Murphy followed 151 HTLV-1–positive and 387 HTLV-2–positive former blood donors for 10 years (5). Compared with uninfected controls, HTLV-positive subjects had significantly more motor and coordination abnormalities. Murphy concluded that HTLV-1 and HTLV-2 infections are associated with a spectrum of neurologic defects beyond those described previously for classic HAM.

Tax, Transcription, Cellular Proliferation, and Transformation

The HTLV-1 Tax oncoprotein induces cellular proliferation, survival, and genetic damage. Nuclear factor-κB (NF-κB) has been described as an important cellular target activated by Tax through both the canonical and noncanonical pathways. Masahiro Fujii (Niigata University, Niigata, Japan) suggested in new findings a specificity of noncanonical NF-κB activation in HTLV-1 pathogenesis. He found that noncanonical activation of NF-κB, as measured by p52 processing from its p100 precursor, is restricted to HTLV-1, but not HTLV-2, Tax. Interestingly, HTLV-1, but not HTLV-2, is oncogenic. Fujii further reported that noncanonical NF-κB activation depends on the PDZ binding motif (PBM) of Tax1 (located in carboxyl-terminal amino acids 350–353).

Following-up on the role of Tax PBM, complete genome sequences from two recently isolated African HTLVs, HTLV-3 (Sara Calattini and Renaud Mahieux, Pasteur, Paris, France) and HTLV-4 (William Switzer, Centers for Disease Control and Prevention, Atlanta, GA), were presented. The data revealed that HTLV-3 Tax retains a PBM that is absent from HTLV-4 Tax. This observation predicts different pathogenic outcomes from HTLV-3 and HTLV-4 infections.

Two presentations addressed Tax and genetic instability. Susan Marriott (Baylor College of Medicine, Houston, TX) reported that Tax represses double-strand DNA repair, which is partly governed by a protein complex containing DNA-protein kinase (DNA-PK). John Semmes (Eastern Virginia University, Norfolk, VA) showed that Tax binds DNA-PK directly and sequesters this factor into nuclear speckles, thus repressing double-strand DNA repair.

Note: The 13th International Conference on Human Retrovirology was held from May 22–25, 2007 in Hakone, Japan.

Requests for reprints: Kuan-Teh Jeang, Laboratory of Molecular Microbiology, National Institute of Allergy and Infectious Diseases, Building 4, Room 306, 9000 Rockville Pike, NIH, Bethesda, MD 20892-0460. Phone: 301-496-6680; Fax: 301-480-3686; E-mail: kj7e@nih.gov.

doi:10.1158/0008-5472.CAN-07-2587

Tax can affect host cell metabolism through transcriptional activation of cellular genes. Jennifer Nyborg (Colorado State University, Fort Collins, CO) found that Tax promotes cyclic AMP–responsive element binding protein (CREB) phosphorylation, increasing the availability of modified CREB for promoter transactivation. Paul Laybourn (Colorado State University) identified a new function of Tax abrogation of H1-mediated repression of p300 coactivator activity. Laybourn also found that Tax decreased histone mRNA levels, arguing that such reduction may contribute to dysregulated expression of many cellular genes. Additional insight into Tax activation of promoters was provided by Nicholas Polakowski and Isabelle Lemasson (East Carolina University, Greenville, NC) who used a chromatin immunoprecipitation assay/microarray (ChIP-on-CHIP) approach to describe direct recruitment of Tax to many cellular promoters.

What are some of these promoters? Cynthia Pise-Masison's [National Cancer Institute (NCI), Bethesda, MD] microarray analyses revealed increased expression in ATL leukemic cells of genes linked to cell cycle progression (e.g., *CDC2, CCN1*), apoptosis repression (e.g., survivin), and tyrosine kinases (e.g., Lyn). Separately, Ralph Grassmann (University of Erlangen-Nuremberg, Erlangen, Germany) and Kuan-Teh Jeang (NIAID) showed altered microRNA (miRNA) expression in HTLV-1–transformed cells, suggesting that Tax also affects/occupies promoters that transcribe oncogenic miRNAs.

Many questions pertaining to *in vivo tax* and virus expression are currently unanswered. Charles Bangham (Imperial College, London, United Kingdom) used deuterated glucose for labeling patients' lymphocytes to check the *in vivo* effect of *tax*/HTLV expression on lymphocyte population dynamics. He saw increased proliferation of $CD4^+CD45RO^+$ and $CD8^+CD45RO^+$ T-lymphocytes in HTLV-1–infected persons compared with controls, with the additional production of 10^{12} lymphocytes per year in the former. The *in vivo* proliferation rate of $CD4^+CD45RO^+$ cells correlated with *tax* expression (measured *ex vivo*), supporting a physiologic role (directly or indirectly) for this viral oncoprotein in the proliferation of infected cells (6).

Functional Contributions from HTLV Accessory Genes

Besides *gag, pol, env*, and *tax*, HTLV encodes *rex* and accessory genes *hbz, p12, p13, p27*, and *p30*. Agnes Lezin (Fort-De-France, Martinique) quantified the expression levels of the HTLV-1 accessory genes in primary cells from HAM/TSP, ATL, and asymptomatic patients. She reported that that *p12, p27*, and *p30* expression was undetectable whereas levels of *tax, hbz*, and *p13* transcripts quantitatively correlated with clinical progression.

HTLV-1 HBZ is unique among viral proteins in being encoded by the minus strand of the provirus. Published studies suggested that *hbz* can function as an RNA and as a protein. At this meeting, Masao Matsouka (Kyoto University, Kyoto, Japan) mapped HBZ proliferative activity to the 5′ end of its RNA. His transgenic mice constructed to express *HBZ* gene driven by the mouse CD4 promoter/enhancer showed increased $CD4^+$ T cells in the spleen with infiltration into the skin and lung. Osamu Isono (Kyoto University) presented evidence that HBZ protein represses c-Jun activity by destabilizing c-Jun and promoting its proteosomal degradation. Jean-Michel Mesnard (Centre National de la Recherche Scientifique, Montpellier, France) had previously published that HBZ protein stimulates JunD activity. Following up on that finding, Sophie Kuhlmann (INSERM, Lyon, France) reported that HBZ/JunD interaction upregulates expression of the *human telomerase reverse transcriptase* gene, potentially explaining elevated telomerase activity in ATL cells.

The p30 protein promotes replication and persistence of HTLV-1 by acting at transcriptional and posttranscriptional levels. Veffa Franchini (NCI) used an infectious proviral clone to show the action of p30 in posttranscriptional gene repression. She showed that deletion of p30 from the provirus increased Tax expression and HTLV-1 replication. Michael Lairmore (Ohio State University, Columbus, OH) followed with data that added complexity to p30 function. He found increased phosphorylation of cell cycle regulators Cdc25C and Chk1 in Jurkat T-cells expressing p30, and p30 association with nuclear γ-H2AX DNA-repair foci. Lairmore proposed a role for p30 in signaling DNA damage (perhaps triggered by retroviral integration).

HTLV-1 p13 and Rex were also discussed at this meeting. Vincenzo Ciminale showed that p13 expression increased mitochondrial reactive oxygen species, influencing the metabolism of the cell by favoring aerobic metabolism, and moderating apoptosis. Patrick Green (Ohio State University) discussed that the phosphorylation status of HTLV-2 Rex at its COOH terminus is important for protein stability and function. Phosphomimetic Rex mutants were shown to be constitutively active, and these Rex mutant viruses displayed increased viral replication both *in vitro* and in inoculated rabbits. However, Rex mutant viruses were similar to wild-type virus in the capacity to immortalize T lymphocytes in culture and persist in infected rabbits.

Immunologic Implications of Viral Infection

Inflammatory lesions in HAM/TSP are associated with the breakdown of the blood-brain barrier. The factors that cause the breakdown of the blood-brain barrier are not known. Philippe Afonso (Pasteur Institute, Paris, France) showed that HTLV-1–infected lymphocytes could induce an increase in both paracellular endothelial permeability and transcellular migration in an *in vitro* model of the blood-brain barrier. The observed changes were accompanied by disruption of intercellular tight junctions and seemed to be mediated by interleukin (IL)–1 and tumor necrosis factor-α.

HTLV-1 Tax induces strong expression of the high-affinity IL-2Rα chain (CD25) on the infected $CD4^+$ T cell. CD25 is also characteristically expressed at a high level on the malignantly transformed $CD4^+$ T cells in ATL. These observations have stimulated considerable interest because certain $CD4^+$ $CD25^+$ T cells, known as regulatory T cells (T_{regs}), can suppress the proliferation and function of other T cells. It is now becoming clear that the intracellular expression of the transcriptional factor FoxP3 in $CD4^+$ T cells is more strongly associated with a T_{reg} phenotype than is CD25 expression, because CD25 is also characteristically expressed on activated T cells. Because of the expression of both CD25 and, in a proportion of cases, FoxP3 in ATL cells, questions have recently been raised whether HTLV-1 preferentially infects or transforms $CD4^+$ $CD25^+$ $FoxP3^+$ T cells (Shimeru Kamihira, Nagasaki University, Nagasaki, Japan) and whether the ATL cells themselves act as T_{regs}: The latter

is an important possibility because ATL is characterized by even more profound immunosuppression than is seen in other leukemias.

Hiroki Yano (Nagoya City University, Nagoya, Japan) tested the ability of ATL cells (identified by a receptor frequently coexpressed on ATL cells, CCR4) to inhibit the proliferation of autologous $CD4^+$ non-ATL cells. In five ATL cases studied, evidence was obtained of a degree of suppression in one case, and suggestive evidence was obtained in one further case. Frederic Toulza (Imperial College, London, United Kingdom) used a simple phenotypic definition of T_{reg} cells, $CD4^+$ $FoxP3^+$, and reported that the percentage of $CD4^+$ $FoxP3^+$ cells in the circulation was negatively correlated with the rate of lysis of autologous naturally infected $CD4^+$ T cells by the patient's $CD8^+$ CTLs. The results suggest that $CD4^+$ $FoxP3^+$ cells play a major role in determining the efficiency of CTL surveillance of HTLV-1. Because there is increasing evidence that the CTL response to this virus determines the proviral load and the risk of inflammatory disease, it is possible that T_{regs} are an important determinant of the outcome of HTLV-1 infection.

Mari Kannagi (Tokyo Medical and Dental University, Tokyo, Japan) reported that immunization of orally infected rats with syngeneic, mitomycin C–treated HTLV-1–transformed cells boosted the cellular immune response to HTLV-1, and that this strengthened immune response was accompanied by a reduction in the proviral load (7). Charles Bangham has evidence for abnormally rapid turnover *in vivo* of both HTLV-1–infected $CD4^+$ T cells and $CD8^+$ T cells (which include the HTLV-1–specific CTLs; ref. 6) with a typical HTLV-1–infected individual turning over an extra 10^{12} lymphocytes per year. Thus, the findings from rats (7) and humans (6) lend weight to the growing evidence that HTLV-1 does not rely solely on latency to persist. Rather, HTLV-1 infection seems to be a highly dynamic equilibrium between persistent viral expression and the immune response.

Therapeutic Approaches to HTLV-1 Infection

Several speakers reviewed various ATL treatment options. Deidre O'Mahony (NCI) presented a phase 1 trial of Splizumab, a monoclonal antibody that binds to CD2 on human T-cells and natural killer cells, in CD2-positive lymphoid malignancies, including aggressive ATL with early encouraging response rates and relatively low toxicities. Lee Ratner (Washington University, St. Louis, MO) reported mixed clinical and virological findings from etoposide, prednisone, vincristine, cyclophosphamide, and doxorubicin (EPOCH) infusional chemotherapy followed by zidovudine and interferon-α. Low levels of viral RNA were seen at the initiation of therapy, but viral RNA levels increased >10-fold in most relapsed cases during therapy. Juan Carlos Ramos (University of Miami, Miami, FL) found that the expression of IRF-4/MUM-1 and c-Rel in the absence of Tax in primary ATL cells was associated with resistance to zidovudine and interferon-α treatment.

Impressive treatment efficacy was seen from reduced-intensity stem cell transplantation (RIST) as reported by Ryuji Tanosaki (National Cancer Center Hospital, Tokyo, Japan). Among 18 patients who received RIST, 14 patients achieved complete remission. Three-year overall survival and event-free survival were 67 ± 12% and 55 ± 12%, respectively. Further explaining why stem cell transplantation is effective for ATL, Nanae Harashima (Tokyo Medical and Dental University) reported that Tax-specific CTL response was recovered [by stimulating peripheral blood mononuclear cells (PBMC) *in vitro* with HTLV-1–infected cells] after stem cell transplantation, suggesting a role for CTL in eliminating Tax-expressing cells and preventing relapse of ATL.

Seishi Ogawa and Toshiki Watanabe (University of Tokyo) described molecular allelo-karyotyping of primary ATL cells using high single-nucleotide polymorphism genotyping microarrays. ATL lymphoma-type genomes from 108 patients showed characteristic copy number profiles and unique patterns of allelic imbalances. Future detailed molecular investigation of these results could reveal novel drug targets for ATL treatment.

For TSP/HAM treatment, Agnes Lézin (Fort-De-France, Martinique) is investigating the use of histone deacetylase inhibitors, valproate, to activate the expression of latent HTLV-1 proviruses *in vivo* and expose the activated infected cells to CTL immune surveillance. Lézin reported that valproate induced a significant reduction of provirus loads (mean 24-fold) in HAM/TSP patients.

Development of Mouse Models for HTLV-1 and ATL

To date, oncogenic potential of Tax in transgenic mice has been intensively studied. However, all extant lymphoid and nonlymphoid tumors in mice have lacked the CD4 surface marker. By contrast, CD4 is present on almost all patient ATL cells. Hideki Hasegawa (National Institute of Infectious Diseases, Tokyo, Japan) had published recently that transgenic mice expressing Tax driven by a lymphocyte-specific protein tyrosine kinase Lck-proximal promoter, targeting immature thymocytes, developed $CD4^-$ $CD8^-$ double-negative pre–T-cell leukemia/lymphoma (8). In new findings using the distal *lck* promoter, Takeo Ohsugi and Toru Urano (Kumamoto University, Kumamoto, Japan) now reported a *tax* transgenic mouse, which developed $CD4^+$ T-cell leukemia (9).

It is popular to use nonobese diabetic severe combined immunodeficient (NOD-SCID) common γ-chain null (NOG) mice for transplantation with human cells. Paola Miyazato (Kyoto University) showed that spread of HTLV-1 infection in human PBMCs transplanted into NOG mice could be blocked by azidothymidine and tenofovir but only in early stages of infection. She discussed that Tax mRNA expression in the infected human cells in NOG mice increased after *in vitro* culture, similar to that seen in human cases. In a related approach, Prabal Banerjee (State University of New York, Syracuse, NY) explanted HTLV-1–infected human $CD34^+$ hematopoietic progenitor cells into NOD-SCID mice. He observed HTLV-1–infected human T cells, B cells, and monocytes/macrophages in transplanted mice. Some of the mice showed proliferation of HTLV-1–infected $CD4^+$ T cell in lymphoid tissues as well as HTLV-1–infected $CD34^+$ cells persisting in the bone marrow and thymus. Banerjee also reported that reconstitution of NOD-SCID mice with HTLV-1 Tax-transduced human $CD34^+$ cells produced proliferating $CD4^+$ T cells.

Future Perspectives

In the 30 years since the description of ATL, much has been learnt about HTLV-1 pathogenesis. Going forward, several important questions remain to be addressed for oncological research on ATL. Will the next years bring clarifying insights into roles contributed by human miRNAs to ATL initiation and progression? Will we learn